Arabian Journal of Chemistry (2023) **16**, 104122

King Saud University

Arabian Journal of Chemistry

www.ksu.edu.sa
www.sciencedirect.com

ORIGINAL ARTICLE

Post Synthetic Modification of NH_2-(Zr-MOF) via Rapid Microwave-promoted Synthesis for Effective Adsorption of Pb(II) and Cd(II)

Humaira Gul Zaman, Lavania Baloo *, Shamsul Rahman Kutty, Muhammad Altaf

Civil and Environmental Engineering Department, Universiti Teknologi PETRONAS, 32610 Seri Iskandar, Perak, Malaysia

Received 5 June 2022; accepted 9 July 2022
Available online 18 July 2022

KEYWORDS

UiO-66-GMA;
Metal-organic framework;
Adsorption: heavy metals;
Microwave-heating

Abstract Excessive heavy metals in the water constitute a health hazard to humans, yet it may be efficiently purified using adsorbents. Herein, for the first time, UiO-66-NH_2 was modified by Glycidyl methacrylate (GMA) via microwave heating method to investigate its potential for adsorption of Pb(II) and Cd(II) metal ions. Synthesized MOF was characterized by TGA, XRD, BET, FE-SEM-EDX, and FTIR. The MOF has a huge surface area of 1144 m^2/g, a mean pore diameter of 2.84 nm, and a total pore volume of 0.37 cm^3/g. The effect of UiO-66-GMA performance was evaluated by investigating the impact of pH (1–9), contact time (0–200 min), initial metal ions concentration (20–1000 mg/L), temperature (25–55 °C), adsorbent dosage (0.5–3 g/L), and co existences of other metals was investigated on Pb(II) and Cd(II) percentage removal. Following an analysis of the adsorption isotherms, kinetics, and thermodynamics, the Temkin isothermal model showed an excellent fit with the adsorption data (R^2 = 0.99). The adsorption process was a spontaneous endothermic reaction and kinetically followed the pseudo-second-order kinetics model. Microwave heating method produced highly crystalline small Zr-MOF nanoparticles with a short reaction time. It promoted the simple yet highly efficient synthesis of Zr-based MOFs, as shown by the reaction mass space-time yield. The adsorption capability of Pb to the presence of several polar functional groups, including as primary and secondary amines, ester, alkene, and hydroxyl groups. This adsorbent is a potential candidate for wastewater treatment due to its outstanding structural stability in acidic and basic solutions, high removal efficiency, and recyclability.

* Corresponding author.
E-mail address: lavania.baloo@utp.edu.my (L. Baloo).
Peer review under responsibility of King Saud University.

Production and hosting by Elsevier

https://doi.org/10.1016/j.arabjc.2022.104122
1878-5352 © 2022 Published by Elsevier B.V. on behalf of King Saud University.

1. Introduction

Heavy metals are a group of pollutants that significantly threaten human health and the environment when their concentrations exceed acceptable levels (Zhang et al., 2020). Heavy metal ion discharge into water bodies has become a major environmental problem all over the globe. Water pollution has recently become a serious issue for many environmental activists and scientists. Trace metal ions have drawn a lot of attention from an environmental perspective due to toxicity, irreversible damages, accumulation in organisms, and non-biological degradation. Trace metals must be removed from water and wastewater before it may be transported and cycled into nature. (Kobielska et al., 2018; Qin et al., 2011). Even though many physicochemical and biological methods for metals adsorption from the contaminated water have been developed (Roushani et al., 2017; Soltani et al., 2021; Wang et al., 2017). Adsorptions superiority over other approaches in the removal of hazardous pollutants, water purification, and the storage of gases is gaining more and more attention each year. Due to the fact that adsorption may be performed at low temperatures, it is less energy-intensive and hence relatively cost-effective (Mahmoud et al., 2021). In recent years, several adsorbent materials for the adsorption of metals have been investigated, including sewage sludge (Phuengprasop et al., 2011), activated carbons (Li Wang et al., 2010), peat (Kalmykova et al., 2008), resins (Liyuan Wang et al., 2010), clays (Bhattacharyya & Gupta, 2007), and biopolymers (Rezakazemi et al., 2014; Roushani et al., 2017; Younas et al., 2020). These adsorbents, in particular, have several basic shortcomings and are suspected to be ineffective at removing trace metals from polluted water in the event of unintentional heavy metal pollution.

MOFs have emerged in the recent decade as a unique form of highly crystalline porous material built by linking ligands with metal ions or metal ion clusters (Mahmoud & Mohamed, 2020; Roushani et al., 2017; Shi et al., 2018; Wang et al., 2015). MOF materials have piqued researchers interest due to its simple and direct ability to modify pore size and shape from microporous to mesoporous scales (Hasan et al., 2016; Liu et al., 2021; Wang et al., 2017). As a result of their wide range of applications, MOFs have recently gained a great deal of interest, including gas adsorption/storage and separation, the catalysis and adsorption of organic molecules, and drug delivery luminescence and electrode materials for nanomaterials (Chavan et al., 2012; Mohamed & Mahmoud, 2020; Nong et al., 2020; Sanchez et al., 2011; Truong et al., 2015; Omar M. Yaghi et al., 1995). As stated previously, MOFs have very promising physical and chemical characteristics for various applications; moreover, their properties may be enhanced via various methods. A few of them include active groups grafting (Hwang et al., 2008), organic linkers modification (Yaghi et al., 2003), impregnating appropriate active materials (Thornton et al., 2009), post-synthetic modification, and ion exchange (Kim et al., 2012).

In 2008, a new family of zirconium (Zr) MOFs, known as UiO MOFs, was developed with unprecedented stability and received much attention. Up to 450 °C, UiO MOFs are thermally inert and chemically resistant to a broad range of organic solvents (Cavka et al., 2008; Feng et al., 2012; Wang et al., 2018; Wißmann et al., 2012). So far, solvothermal methods have been used to synthesize MOFs, which require a long reaction time and a lot of energy. As a result, developing more cost-effective and environmentally friendly synthesis routes is of great interest to the scientific community. Another method for synthesizing MOFs is microwave-assisted synthesis. In this method, dielectric heating produces heat internally inside the reaction medium rather than transported to the medium from outside sources (Klinowski et al., 2011; Tannert et al., 2018). As a result, homogeneous and intense heating can be initiated under microwave irradiation, enabling MOF nucleation and crystal formation.

To make MOFs applicable in various industries, a rapid and inexpensive synthesis process that reduces reaction time and adjusts crystalline size is needed (Atia et al., 2005). UiO-66 MOF was recently synthesized using a microwave heating approach with a 120 minute of reaction time and a yield of about 90%. Further research revealed that the rapid nucleation caused by microwave irradiation often reduced crystal size. UiO-66 nanoparticles synthesized (100 nm) via microwave heating were four times smaller than that produced by traditional heating (about 400 nm).

In recent years, polymers have been employed to increase MOF porosity, and enhance MOF performance in specific applications (Lin Wang et al., 2010; Xiong et al., 2018). MOF-polymers have received much attention as polymers materials are promising for their high uptake capacity, excellent selectivity, and better stability (Dou et al., 2013). Glycidyl methacrylate is a polymer with excellent mechanical strength, acid and basic resistance, and a high epoxy group reactivity (Atia et al., 2005). Additionally, its epoxy group may covalently react with a ligand in a single chemical step (Yin et al., 2017; Yuan et al., 2017). To increase the range of uses for ordinary polymers, a chelating group must be added. Thus, in the present study, the amino group of UiO-66-NH_2 was post synthetically modified and functionalized with GMA as presented in Fig. 1.

The parent MOF's polarity and porosity structure may be altered by adding functional groups like hydroxyl, alkene, and ester to the GMA structure. In addition, the alkene group on the UiO-66-GMA surface allows for post-synthetic alterations by radical polymerization techniques. For the first time in this study, Ui0-66-GMA was synthesized at different reaction times (5, 10, 15, and 30 mins) via the microwave heating method, and removal efficiency for the adsorption of metals was investigated. The microwave heating method produced MOF crystals only after 5 min of reaction time, whereas the conventional approach, i.e., (solvothermal) requires 24 h and 30 min to have high-quality crystals. It is an easy method to produce highly crystalline small Zr-MOF nanoparticles with a short reaction time. This heating method has addressed the key limitation of conventional synthesis methods and has environmental solid application potential for the remediation of waste effluent-containing metals. To date, UiO-66-GMA removal efficiency for metal adsorption has not been investigated. Synthesized MOF was characterized by BET, SEM-EDX, TGA, XPS, FT-IR, and XRD to examine the structural properties. The UiO-66-GMA was used as an adsorbent to remove Pb(II) and Cd(II) metal ions from water. The effects of contact time, pH, adsorbent dosage, initial metal ions concentration, and temperature were carefully examined. In addition, structural stability, selectivity, reusability, adsorption kinetics, isotherms, and adsorption mechanisms were investigated. Overall, this research presents that synthesized MOF has the advantages of high selectivity and a large adsorption capacity.

2. Experimental

2.1. Chemicals

All reagents used in this research, including Dimethylformamide 99 % (DMF), 2-aminoterephthalic acid (99 %,) and Zirconium chloride ($ZrCl_4$), were acquired from Sigma-Aldrich. Moreover, Lead nitrate ($Pb(NO_3)_2$), Cadmium nitrate $Cd(NO_3)_2$, Copper nitrate $Cu(NO_3)_2$, Chloroform (99 %), Tetrahydrofuran (THF, 99.5 %), and Glycidyl Methacrylate (GMA, 97 %) were acquired from Merck and used without further purification.

2.2. MOF Synthesis

Microwave synthesis of UiO-66-GMA MOF nanoparticles was conducted in a microwave oven for reaction times of 5, 10, 15, and 30 min (Glanz P70D20SP-DE, Shenzhen, China). In all experiments, the microwave output power was kept con-

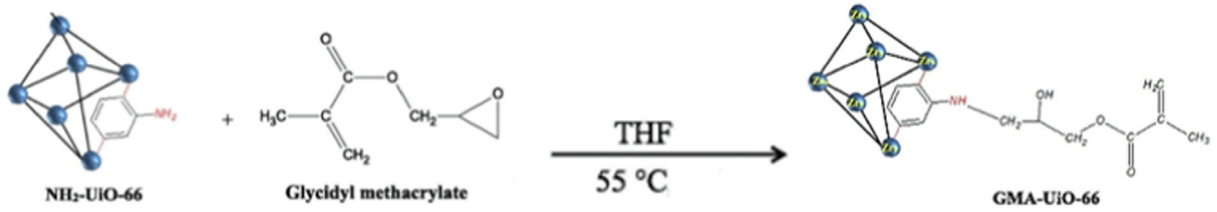

Fig. 1 UiO-66-NH_2 PSM with GMA (Molavi et al., 2018a).

stant at 800 W. UiO-66-NH_2 (60 mg) nanoparticles were dissolved in a solvent THF (5 mL) and sonicated for 20 min. After that, 0.22 mL GMA was added and placed in a 200 mL boiling flask. After that, the crucible was placed in a microwave oven. Following microwave irradiation for the desired reaction time (5 min for sample A, 10 min for sample B, 15 min for sample C, and 30 min for sample D), the nanoparticles were collected by centrifugation at 4000 rpm for 10 min, repeatedly washed with THF, and then sonicated in chloroform for 10 min to remove any unreacted GMA before being soaked in chloroform for two days. Finally, the yellowish nanoparticles (UiO-66-GMA) were vacuum-dried for one day at 50 °C (Molavi et al., 2018a; Molavi et al., 2018d). Based on Zr, the yield of Ui0-66 GMA MOF for samples A, B, C, and D was calculated to be 59.22 %, 63.31%, 74.92 %, and 82.77%, respectively. Characterization analysis of Ui0-66-GMA, including XRD, TGA, FE-SEM, and FT-IR, are present in Section 3.1.

2.3. Adsorption Performance Evaluation

2.3.1. Stock Solution Preparation

Stock solutions were prepared to imitate typical aqueous solutions containing Pb(II), and Cd(II) metal ions by dissolving the required quantity of metal salts i.e., lead nitrate, and cadmium nitrate in a 1L of distilled water. A 1000 ppm stock solution for both metals and varied concentrations (20–1000 ppm) were obtained by serial dilution to investigate the effects of initial metal concentration on removal efficiency.

2.3.2. Adsorption Study

In all the batch tests, adsorption of Pb(II) and Cd(II) was studied by varying the contact time, adsorbent dose, temperature, initial metal ion concentration, and pH of the solution. Synthesized MOF nanoparticles were added to a Pb (II) and Cd(II) solution (25 mL). All batch tests were performed on a hot plate with a magnetic stirrer and a beaker with 50 mL of solution. The solution pH was adjusted by adding 0.1 M NaOH or 0.1 M HCl. The samples were maintained at 25 + 1 °C using a 220 rpm stirrer. Following the stirring procedure, samples were collected, filtered using a 0.45 m syringe filter (Whatman No.1, 0.45 µm), and then analyzed using Atomic absorption spectrophotometer (Spectra model AA-20) determine the adsorbed metals concentration. The percent removal efficiency (R%) of the adsorbed metal ions at time t (min) was determined by Eq.1.

$$\%\,R = \frac{C_i - C_t}{W} \times V \tag{1}$$

where, C_i and C_t denote the initial and final concentrations of Pb(II) and Cd(II) respectively.

W = amount of the adsorbent (mg).
V = volume of solution (mL).

2.4. Kinetic Study

Pseudo-first order (PFO), pseudo-second-order (PSO), and intraparticle diffusion kinetic models were used to evaluate the adsorption mechanism of Pb(II) and Cd(II) metal ions by UiO-66-GMA. In batch experiments, UiO-66-GMA (40 mg) was dissolved in 50 mL of metal ion solutions (100 mg/L). After stirring for a particular time period (20–360 min), the adsorbent nanoparticles were removed using a centrifuge machine (Ahmadijokani et al., 2020).The results of each kinetic adsorption experiment were verified three times to ensure accuracy (Molavi et al., 2018e).

2.5. Isotherm Study

The Langmuir, Freundlich, and Temkin isotherm models were used to analyse experimental data from adsorption equilibrium investigations. The adsorption of Pb (II) and Cd(II) onto UiO-66-GMA have been investigated by dissolving 8 mg MOF in metal ion solution (10 mL) with varying concentrations at different temperatures. Isotherms at various temperatures are essential for assessing adsorbent adsorption behavior toward adsorbate molecules and predicting the favourability of the adsorption process.

Isotherm models acquired by fitting experimental results to Freundlich, Langmuir, and Temkin are presented in Eqs. (2), (3), and (4), respectively.

$$\mathbf{q_{eq}} = \frac{\mathbf{q_{max}bC_{qe}}}{1 + \mathbf{bC_{eq}}} \tag{2}$$

whereas, *qeq* is uptake metal capacity at equilibrium, Ceq concentration of the metal ion.

$$q_{eq} = K_f C_{eq}^{\frac{1}{n}} \tag{3}$$

where n and K_f are the Freundlich constants linked to the sorbent's adsorption capacity and intensity, respectively.

$$\mathbf{qe} = \frac{\mathbf{RT}}{\mathbf{b}} \ln \mathbf{KT} + \frac{\mathbf{RT}}{\mathbf{b}} \ln \mathbf{Ce} \tag{4}$$

where b represents the Temkin constant which is related to the heat of sorption ($Jmol^{-1}$), and KT(Lg^{-1}) is the Temkin isotherm constant.

PFO (Eq. (5)), PSO (Eq. (6)) and intraparticle diffusion (Eq. (7)) kinetic models are used to express the mechanism of metal ions removal by Ui0-66-GMA.

$$\log(q_e - q_t) = \log(q_e) - K_1 t \tag{5}$$

where qe and qt represent uptake of metal uptake at time t respectively, and $k1$ is the constant.

$$\frac{t}{qt} = \frac{1}{qek2} + \frac{1}{qe}t \quad (6)$$

where, qe and qt represent uptake of adsorbate at equilibrium and at time t respectively, and $K2$ is the constant.

$$qt = Kdt^{0.5} \quad (7)$$

where qt is the amount of adsorbent on the surface of the adsorbent at time t (mg g^{-1}), Kd is the intraparticle rate constant (mg (g min0.5)$^{-1}$), and t is the time (min).

2.6. Multi-Metal-Ions Adsorption Study

The removal effectiveness of UiO-66-GMA for each metal ion in a combination of the two and three metal ions were examined to analyze the impact of metal ion coexistence. Metal ions in binary and ternary solutions were removed by adding GMA-UiO-66 (8 mg) to a 10 mL solution containing 100 mg/L of various metal ions. The mixes were mixed for 6 h at room temperature. The residual amount of each metal ion in the mixture was measured using atomic absorption spectroscopy, and removal efficiency was calculated using Eq.1.

2.7. Stability Study

A MOF nanoparticles capacity to withstand acidic and basic solutions is essential for long practical applications. The structural stability of the samples was tested over 24 h in the presence of HCl (pH 1) and NaOH (pH 14) solutions. In brief, 100 mg UiO-66-GMA nanoparticles were mixed with 50 mL of acidic or basic solutions and stirred at room temperature for 24 h. Following that, the nanoparticles were collected, washed with chloroform, and dried at 60 °C. Finally, the XRD diffractograms of acid/base treated adsorbents were compared to assess structural stability (Ahmadijokani et al., 2021; Molavi et al., 2018b).

3. Results and Discussion

3.1. Uio-66-GMA Structural Characterization

GMA nanoparticles were synthesized by microwave irradiation method for different reaction times of 5, 10, 15, and 30 min as shown in Fig. 2. The XRD patterns of Ui0-66-GMA MOF show four distinctive peaks at 2θ values of roughly 7.42°, 8.5°, 12.1° and 25.7. The crystalline structure of the synthesized MOF matches well with the previously reported patterns in the literature, as shown in Fig. 2 (Kopinke et al., 2018). Microwave irradiation produces crystals only after 5 min of reaction time, whereas the conventional approach requires 24 h and 30 min to produce high-quality crystals. Compared to conventional heating methods, the MOF crystals synthesized by this method are substantially smaller, ranging from 150 to 200 nm in size (Chavan et al., 2012). Surface area of the UiO-66-GMA MOF is not affected when compared with the conventional heating method. Furthermore, MOF nanoparticles have no obvious change with increasing the irradiation time from 5 to 30 min. It is an easy, low-cost, and environmentally friendly approach to producing

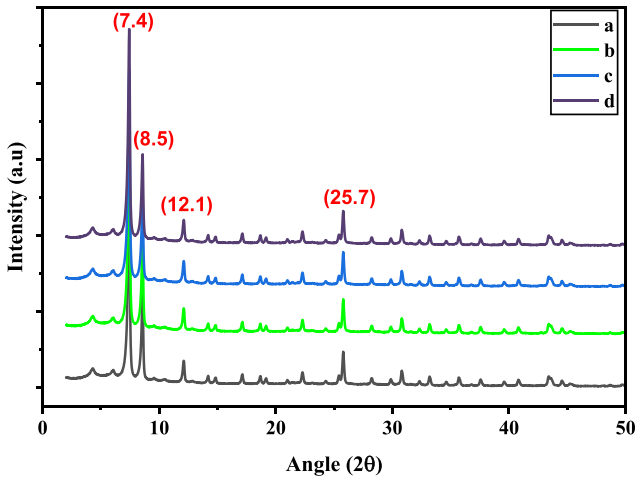

Fig. 2 XRD patterns of the synthesized (a) Ui0-66-GMA sample (a–d) for 5, 10,15 and 30 min.

highly crystalline Zr-MOF nanoparticles. Also, XRD patterns of the samples showed broad Bragg reflections, indicating the presence of small-sized crystals, which is consistent with the FE-SEM and TEM results. Yield of Ui0-66-GMA MOF crystals for samples A, B, C, and D were calculated to be 69.84%, 78.34%, 88.12%, and 93.94%, respectively, based on Zr.

The average crystallite size of the UiO-66-GMA was calculated according to the Debye Scherer formula, using Eq. (8) and shown in Table 1.

$$L = \frac{Ks\lambda}{(\cos\varnothing)T} \quad (8)$$

FT-IR plots represent the chemical composition of UiO-66-GMA and UiO-66-NH_2 as shown in Fig. 3. In the UiO-66-GMA spectra, the peak observed at 3389 cm^{-1} is associated with the —NH_2 group and the 2-aminoterephthalic acid (Abid et al., 2013; Rallapalli et al., 2011; Saleem et al., 2016). The principal characteristic peaks of UiO-66-GMA belong to C—H stretching vibrations (2883-2937 cm^{-1}), Zr metal clusters coordinated through the organic ligand, and C—O—C bond stretching vibrations of the terephthalic acid ligand (at 1584 cm^{-1}), benzene ring's vibration (at 1400 cm^{-1}). The peaks observed at 566 cm^{-1} was assigned to Zr—O bond absorption, indicating the coordination between the $ZrCl_4$ and 2-ATA. The bands at 1039 cm^{-1} correspond to C—O stretching (Dennis et al., 2016). The characteristic peak at 1715 cm^{-1}, which is connected to the ester carbonyl stretching of UiO-66-GMA and indicates that GMA has been successfully bonded to the MOF, is one of the most distinguishing and immediately recognizable peaks in an IR spectrum. The FT-IR data represented the literature well.

Thermogravimetric analysis (TGA) and differential thermogravimetric analysis (DTG) were used to study the thermal stability of Ui0-66-GMA. A heating rate of 10 °C/min was used for the TGA and DTG analyses at temperatures between 28.89 and 793.28 °C, as shown in Fig. 4. Ui0-66-GMA MOF shows three stages of weight loss followed by three endothermic peaks in the DTG curve. Decomposition of GMA may begin at lower temperatures than MOF and thus results in a wide DTG peak. The first noticeable weight loss step at 100 °C corresponds to dehydration (J. Zhu et al., 2019). The

Table 1 Structural properties of the synthesized UiO-66-GMA.

Sample	2 θ (°)	FWHM	d-spacing (nm)	Crystallite size (nm)
Ui0-66-GMA	25.7, 12.1, 8.5,7.4	0.1279	3.16426	66.94

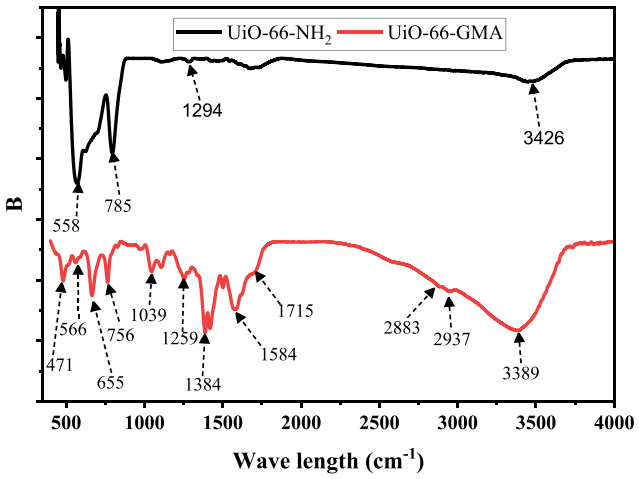

Fig. 3 FTIR spectra of the synthesized UiO-66-NH_2 and UiO-66-GMA.

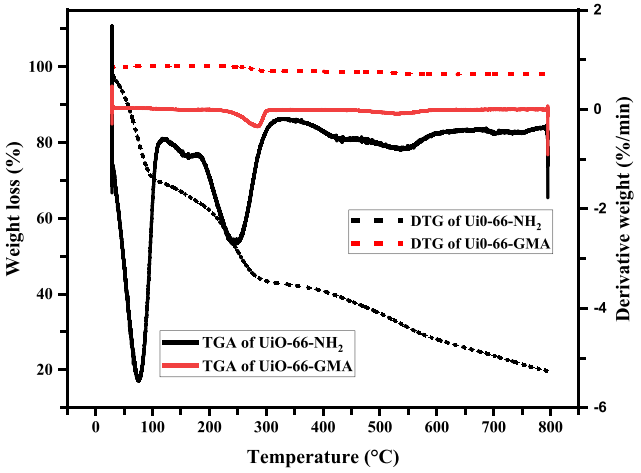

Fig. 4 TGA and DTG analysis of Ui0-66-NH_2 and UiO-66-GMA.

second loss of around 285 °C may be due to the loss of solvent (DMF) molecule residues, which were not exchanged by chloroform (Molavi et al., 2018a; Molavi et al., 2018d). The third board DTG peak at 530 °C and corresponding weight-loss in the T.G. curve is attributed to the GMA group degradation grafted on the MOF surface and probably to the decomposition of the MOF framework (Abid et al., 2013; Molavi et al., 2018d). From the TGA analysis, it is evident that synthesized MOF, is thermally stable up to 530 °C. The ultimate residue ash value of UiO-66-NH_2 at temperatures over 600 °C is greater than that of UiO-66-GMA, principally owing to the inclusion of GMA in the modified MOF. As a result, the difference in residue ash between MOFs is due to the degree of GMA functionality.

Field emission scanning electron microscopic (FE-SEM) and transmission electron microscopy (TEM) were used to examine the microstructure of synthesized UiO-66-GMA. As shown in Fig. 5 (a), UiO-66-GMA images have the same morphology and surface roughness. The morphology of this material is similar to that found in the literature (Molavi et al., 2018d; Yang et al., 2019; Ramezanzadeh et al., 2021a). TEM images are shown in Fig. 5 (b). The obtained nanocrystals regularly have spherical microcrystals with 150–200 nm sizes.

XPS measurements have been carried out to ascertain the surface chemical state of the synthesized MOF. As presented in Fig. 6a, the XPS survey spectrum confirms the existence of C, O, N, and Zr in the synthesized MOF, which corresponds to the analysis of EDS indicating full Zr, C1s, N1s, and O1s spectra scan. In XPS spectra of UiO-66-GMA MOF, notably carbon and oxygen peaks were much higher which corresponds to analysis of EDS. The Zr 3d spectrum peaks at 182.7 eV were attributed to Zr═O bond and the peak at at 400.3 eV corresponds to N1s was possibly assigned to the interaction between the proton and the amidogen (eNH_3^+) (Chen et al., 2015; He et al., 2019). Fig. 6(b) shows the curve fitting results for O1s binding energy at 530 and 536.57 eV were given to C─O, and carboxyl oxygen functional groups. As shown in Fig. 6c, the C 1s spectrum can be divided into four peaks: C═C, C─N, C─C, and C═O, corresponding to 284.5, 285.2, 285.9, and 288.8 eV, respectively (Sarker et al., 2018).

The chemical composition of the synthesised UiO-66-GMA was confirmed by EDX analysis as shown in Fig. 5(c) and the data presented in Table 2. The presence of oxygen (O), carbon (C), nitrogen (N), and Zirconium (Zr) prominent diffraction peaks are confirmed in Fig. 5C, which are basic building units of UiO-66- and similar to the result reported by the previous literature (Fiaz & Athar, 2020; Mansouri et al., 2021). Due to their exceptional purity and single-phase development, these samples had no additional impurity peak in image. Furthermore, the Zr concentration estimated by ICP-OES reduces when GMA is introduced to UiO-66-NH_2.

The specific surface area, mean pore diameter, and total pore volume of the synthesized MOFs were evaluated by BET through N_2 adsorption/desorption isotherms at 77 K. The obtained results in comaprsion with the previous studies are summarized in Table 3. The surface area, mean pore diameter, and total pore volume of 1144 m^2/g, 2.84 nm, and 0.37 cm^3/g were calculated for the UiO-66-GMA NPs, respectively. The BET surface area of UiO-66-GMA is the same as, or slightly larger than, the value previously reported (Tian et al., 2018; J. Zhu et al., 2019). Surface modification of UiO-66-NH_2 may have partially blocked the pores due to the introduction of bulky GMA groups on the surface. The parent MOF, which had a pore diameter of 3.95 nm, exhibited a shift of 2.84 nm after functionalization with GMA, with a difference of 1.1 nm. MOFs with an increased surface area verify small materials, a significant number of pores, and pore volume. On activation, solvent plays a significant role in elim-

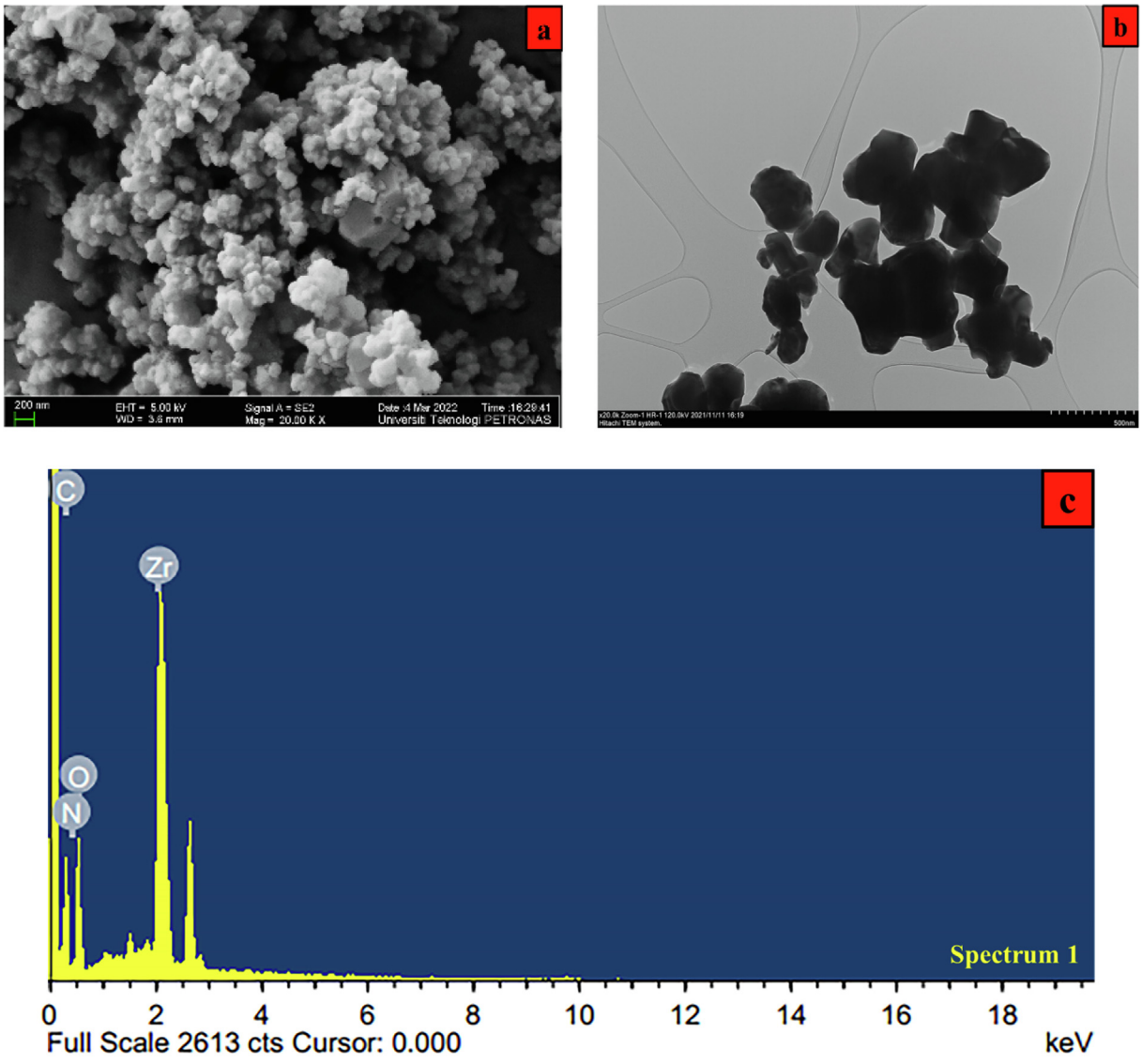

Fig. 5 UiO-66-GMA (a) FE-SEM (b) TEM and (c) EDX.

inating impurities, which results in a large surface area. UiO-66-GMA had pore diameters less than 2 nm, indicating mesoporous structures.

3.2. Adsorption study

3.2.1. Effect of pH

For metal adsorption, the initial pH value of the adsorbent is an important parameter because it affects the chemical speciation of the metal ions in the adsorbate and the protonation of polar functional groups on the adsorbent surface. Consequently, investigating the impact of solution pH on the removal efficiency of UiO-66-GMA for Pb(II) and Cd(II) ions is worthwhile. For all adsorbate ions, the removal effectiveness of the UiO-66-GMA is lower at low pH values and increases with increasing pH, as shown in Fig. 7(a). The presence of many hydrogen ions in highly acidic conditions causes the amine groups of adsorbents to be protonated, as illustrated in Scheme 1. Total surface charge becomes positive, preventing the formation of bonds between positively charged metal ions and the adsorbents' surface. Moreover, under acidic conditions, H_3O^+ ions compete with other adsorbate ions for active sites that are unoccupied. For these phenomena, the removal efficiency of metal ions at low pH values declines significantly. The charge state of the UiO-66-GMA was investigated further using zeta potential measurements across a broad pH range, as shown in Fig. 6(b). The MOF showed positive zeta potential in the acidic pH range, which flipped to negative zeta potential at pH values greater than 5.5. This supports the hypothesis of protonated MOF cages at acidic pH and the formation of neutral to negatively charged particles in neutral/basic pH. The electrostatic repulsion between the positively charged adsorbent and metal ions increased when the pH of the metal ions solution was lower than the isoelectric point of the adsorbent, resulting in a decrease in the removal efficiency of metal ions. In other words, as shown in Scheme 1. when the pH of the metal ions solution is greater than the isoelectric point of the adsorbent (pH > isoelectric point of UiO-66-GMA), the adsorbent's surface charge or zeta potential becomes negative,

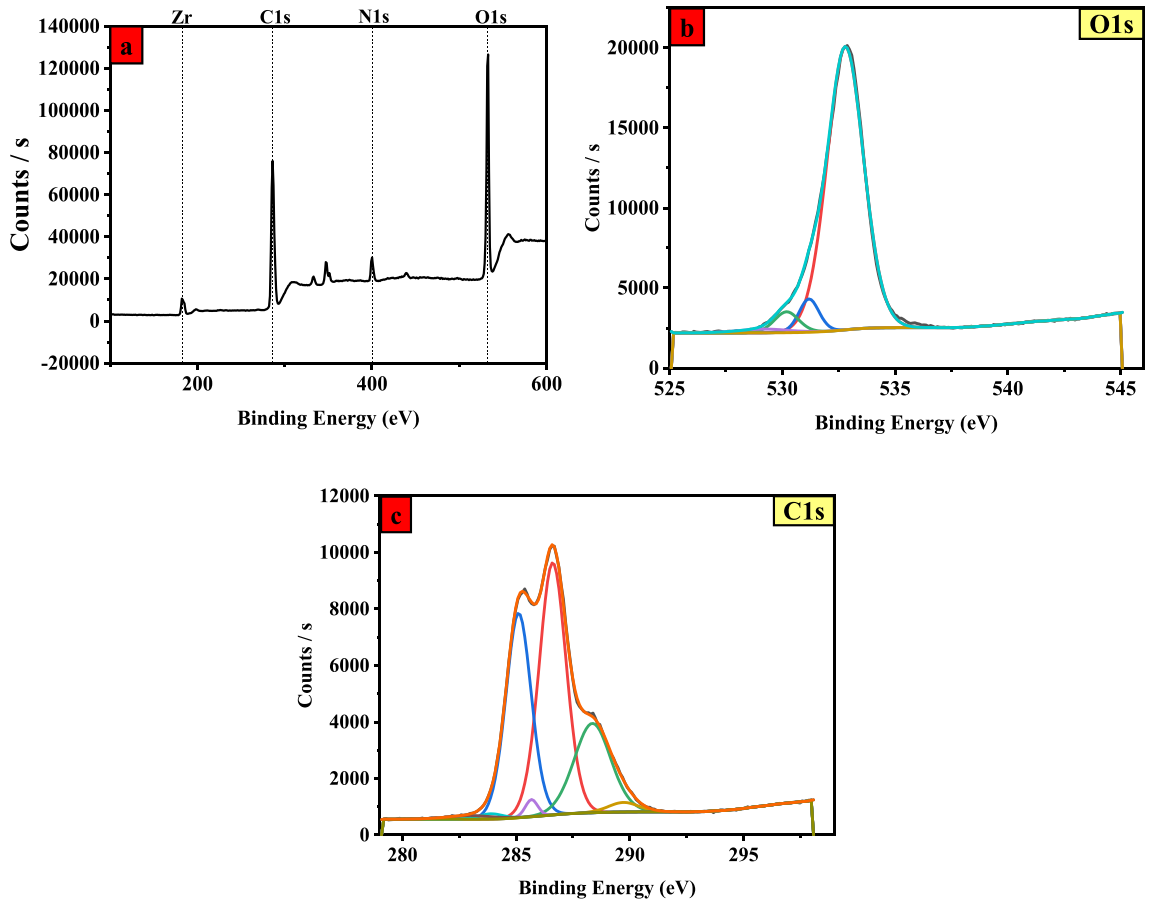

Fig. 6 XPS spectrum of MOF (a) Full scan (b) O1s spectra (c) C1s spectra.

Table 2 Elemental analysis of the synthesized UiO-66-NH_2, and UiO-66-GMA.

MOFs	Atomic (%)			
	C	O	N	Zr
UiO-66-NH_2	25.28	46.60	8.54	19.58
UiO-66-GMA	54.31	33.14	4.49	8.06

Table 3 BET analysis comparison for UiO-66-NH_2 and UiO-66-GMA.

MOFs	BET Surface Area (m^2/g)	Total pore volume (cm^3/g)	Mean pore diameter (nm)	Reference
UiO-66-NH_2	576	0.42	2.99	(Molavi et al., 2018a)
	710	0.12	2.64	(Wu et al., 2018)
	987	0.51	–	(Zhu et al., 2019)
	977	0.57	–	(Tian et al., 2018)
	822	0.23	0.214	(Cao et al., 2018)
	963.8	0.442	–	(Mansouri et al., 2021)
	826	0.31	0.45	(Nik et al., 2012)
	650	0.24	0.51	(Nik et al., 2012)
	1127	0.48	3.95	This study
UiO-66-GMA	568	0.40	2.85	(Molavi et al., 2018a)
	1144	0.37	2.84	This study

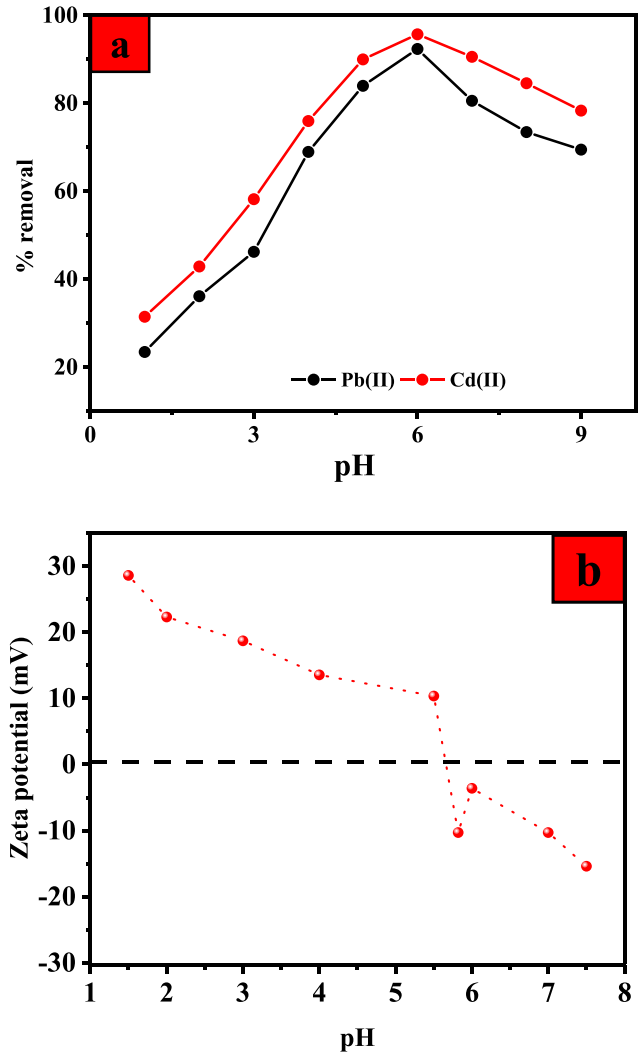

Fig. 7 Effect of solution pH (a) on the Pb(II) and Cd(II) removal efficiencies onto UiO-66-GMA (b) on the zeta potential of UiO-66-GMA.

and the electrostatic attraction between the negatively charged adsorbent and metal ions rises, increasing the removal efficiency of metal ions. Since metal ions are more readily adsorbed to surfaces with high pH values, electrostatic attraction enhances the effectiveness of metal ion removal. Another factor that increases the effectiveness of these metal ions removal is the precipitation of metal hydroxides at higher pHs (Carpio et al., 2014; Demiral & Güngör, 2016; Nyairo et al., 2018; Yan et al., 2018). Furthermore, these findings show that treating the adsorbents with acidic solutions allows UiO-66-GMA nanoparticles to regenerate (Badruddoza et al., 2013). Based on the findings, the ideal solution pH for Pb(II) and Cd(II) removal was predicted to be 6; thus, all further adsorption experiments were performed at this pH value. Below pH 7 Pb (II) and Cd(II) ion, the dominant species was free and primarily involved in the adsorption process. Above pH 7, lead and Cd ions began to precipitate as Pb $(OH)_2$, and $Cd(OH)_2$, which was confirmed by Stephenson and Mishra (Hussain Qaiser et al., 2019; Mishra et al., 2013). At higher pH (> pH 7), the adsorption decreases due to the formation of soluble hydroxy complexes. The pH of the solution had the greatest impact on the adsorption of Pb (II) and Cd (II) ions.

3.2.2. Effect of time

Fig. 8 shows the adsorption capacity of Pb(II) and Cd(II) ions to adsorb on UiO-66-GMA as a function of contact time. The removal efficiency of all metal ions was found to be enhanced when the contact time increased. Pb(II) and Cd(II) ions were quickly adsorbing onto the surface of UiO-66-GMA owing to its number of empty adsorption sites and the high concentration gradient. Adsorption capacity increased slowly over time because of the fast mobility of metal ions inside the MOFs structure, which caused limited intra-specific diffusion. It was observed that increasing contact time enhanced the removal efficiency of all metal ions. The adsorption of Pb(II) and Cd(II) ions was rapid in the first stage due to the abundance of unoccupied adsorption sites on the surface of UiO-66-GMA and the strong concentration gradient. This happened because of the rapid movement of metal ions inside MOFs structure and has a great impact on adsorption capacity to increase slowly with time, resulted in low intra-particular diffusion (Molavi et al., 2018c; Yan et al., 2018). The second step was rather slow due to adsorbate ions occupying a fraction of active sites. It's worth noting that equilibrium states were attained after the saturation of active sites (Badruddoza et al., 2013). The adsorption rate was Cd(II) > Pb(II), as shown in Fig. 4, which might be related to differences in hydrated radius, electronegativity, acid-base characteristics,

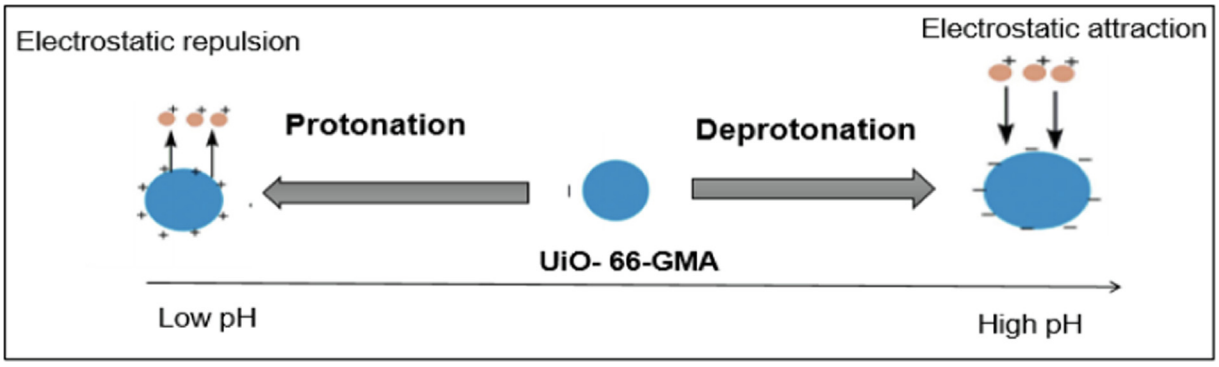

Scheme 1 Schematic impact of solution pH on the UiO-66-GMA surface charge.

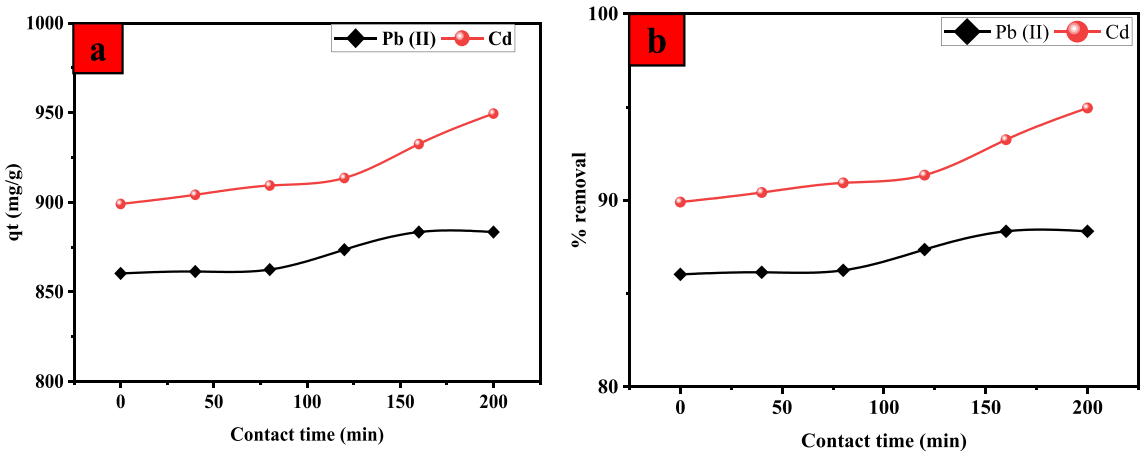

Fig. 8 Effect of contact time on (a) the adsorption capacity and (b) removal efficiency of Pb(II) and Cd(II) onto UiO-66-GMA.

and affinity of UiO-66-GMA. According to the hard-soft-acid-base (HSAB) theory, the amine group acts as a soft base, the Cd(II) ions act as a soft acid, and the Pb(II) ions act as intermediate acids (Hur et al., 2015; Jiao et al., 2016; Zhang et al., 2020).

3.2.3. *Effect of dose*

Another important parameter that influences the removal efficiency is the adsorption dose. Fig. 9 presents Pb(II) and Cd(II) adsorption at the adsorbent dose, ranging from 0.5 to 3 g/L. Adsorption capacity values first increased and then reduced with an increase in adsorbent dose. By increasing the adsorbent dose, gradually the adsorption sites declined between adsorbent and metal ions, and therefore the removal efficiency increases. However, at higher adsorbent dosages, a decrease in removal efficiency may be expected due to the aggregation of adsorbent particles, leading to a reduction in the available vacant sites. Therefore, finding the optimal adsorbent dosage is important to maximize adsorption efficiency. The results showed that increasing the UiO-66-GMA dose significantly increased removal efficiency owing to a larger ratio of active sites to metal ions.

3.2.4. *Effect of initial metal ions concentration*

The adsorption of Pb(II) and Cd(II) metal ions onto UiO-66-GMA was investigated in the range of 20–1000 mg/L, as shown in Fig. 10. By increasing the initial concentration of Pb(II), and Cd(II) metal ions concentration, the adsorbents capacity to chelate with the metal ions was increased, making it clear that the metal ions adsorption rate was increased. As metal ions concentrations increased, the active sites in the Ui0-66-GMA adsorbent became saturated, however this had only a small impact on the adsorption capacities of Pb(II) and Cd(II) from aqueous solution (Jamshidifard et al., 2019).

3.2.5. *Effect of temperature*

The adsorption of Pb(II) and Cd(II) was investigated under various temperatures ranging from 25 to 55 °C. It is obvious from Fig. 11 that Pb(II) have the greatest capacity for a GMA-functionalized MOF at 30 °C. At lower temperatures (25–30 °C), capacity values first increased and later decreased (30–55 °C), which signifies the endothermic nature of the

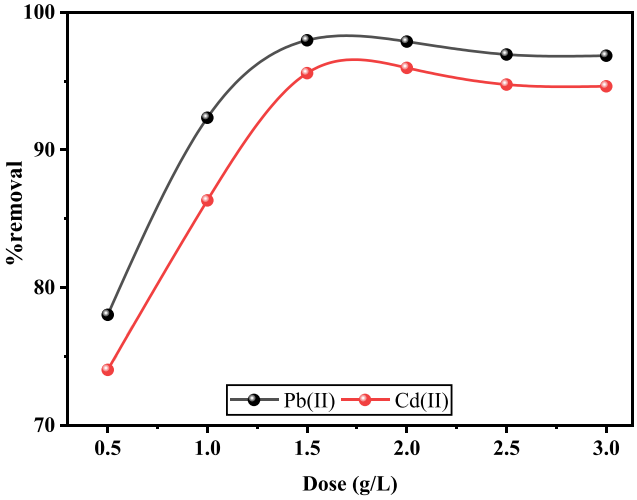

Fig. 9 Effect of adsorbent dose on the removal efficiency of Pb (II), and Cd(II) onto UiO-66-GMA.

adsorption process due to chemical interactions between the Pb(II) and Cd(II) metal ions and the MOF. The weakening of adsorptive forces between the activities of the adsorbent and Pb(II) ions might explain the reduction in adsorption as temperature rises (Akpomie et al., 2012; Guilane & Hamdaoui, 2016; Wang et al., 2017). The capacity of Cd(II) changed with temperature, initially rising significantly (20–30 °C) and then dropping somewhat (30–35 °C) as the temperature increased. From 35 to 55 °C, the Cd(II) capacity increased. However, the decrease in adsorption capacity with the increase in temperature is pointing towards desorption at a higher temperature. In addition, it also indicates that it requires less heat to transfer the Cd(II) ions from the aqueous solution to the solid surface. This resulted in ratifying the metal adsorption mechanism on UiO-66-GMA as a physical process. A similar study was reported by K. Wang et al. (2017) for the adsorption of Pb(II) and Cd(II) ions onto MOF.

3.3. *Adsorption kinetics*

The adsorption of Pb(II) and Cd(II) metal ions onto UiO-66-GMA is investigated using the PFO, PSO, and Temkin kinetics

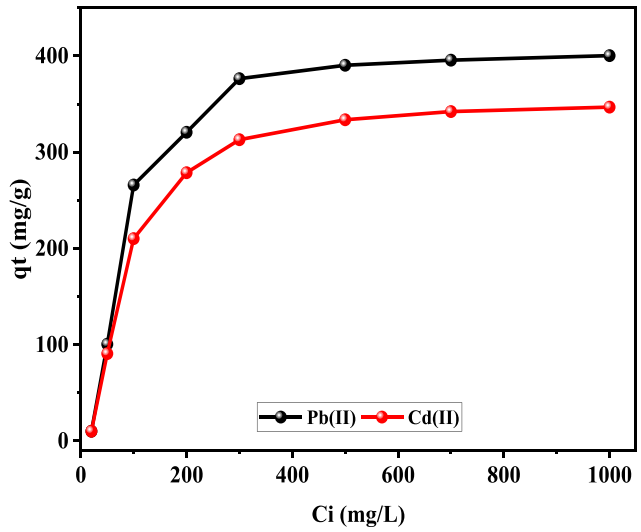

Fig. 10 Effect of initial concentration on the removal efficiency of Pb (II), and Cd(II) onto UiO-66-GMA.

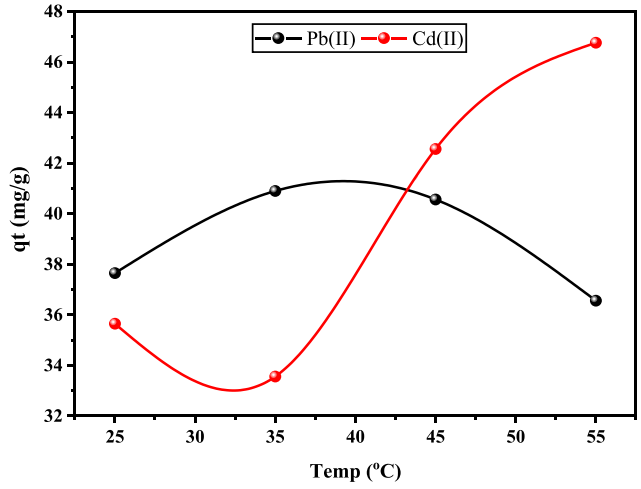

Fig. 11 Effect of temperature on the removal efficiency of Pb (II), and Cd(II) onto UiO-66-GMA.

models with varying contact times. Fig. 12(a) and (b) shows linear plots of the linearized forms of the PFO, PSO and Temkin along with the correlation coefficients and adsorption capabilities; listed in Table 3. The observed (qe) and predicted (qt) values for Pb(II) and Cd(II) metal ions adsorption and PFO show that the limited phase of the adsorption process is not well connected with its reversibility. PFO models show how ions are physically absorbed and how many active sites are available on the adsorbant's surface. Therefore, the results indicate that the PFO model is not appropriate for determining the kinetic mechanism of adsorption of Cd(II) and Pb(II) ions onto UiO-66-GMA. In this study, the PSO kinetic model has a high R^2 value, which is compatible with the adsorption results for Pb(II) and Cd(II). This implies that valency forces and electron sharing or exchange between adsorbent and adsorbate may be the rate-limiting phase in chemical sorption or chemisorption. Several studies in the literature have revealed that the PSO kinetics model offered the best fit for experimental data, including the adsorption of Cd(II) and Pb (II) ions (Vasconcelos et al., 2007; Wu et al., 2001). With a low adsorbent concentration, a pseudo-first-order model is an acceptable adsorbate. The observed (qe) and predicted (qt) values for Pb(II) and Cd(II) metal ions adsorption and PFO show that the limited phase of the adsorption process is not well connected with its reversibility. PFO models show how ions are physically absorbed and how many active sites are available on the adsorbant's surface. As a result, chemical adsorption is predicted to be the rate-controlling step in the adsorption removal of Pb(II) and Cd(II) ions onto UiO-66-GMA(Zhang et al., 2020). Chemical adsorption is often dominated by covalent interactions between active sites and metal ions and electron exchange and sharing. In this study, the PSO kinetic model has a high R^2 value of 0.99, which is compatible with the adsorption results for Pb(II) and Cd(II).This implies that valency forces and electron sharing or exchange between adsorbent and adsorbate may be the rate-limiting phase in chemical sorption or chemisorption. The intraparticle diffusion model for the adsorption of Pb(II) and Cd(II) onto UiO-66-GMA MOF is presented in Fig. 12Sc. The line between uptake (qt) and the square root of time (t0.5) shows that intraparticle diffusion is the rate-controlling step in adsorption systems, as shown in Fig. 12c. Thus, intraparticle diffusion is the primary adsorption process while ion diffusion is the rate limiter (Kopinke et al., 2018; Wang et al., 2008). Four mechanisms are involved in the transport of porous adsorbents: solution-phase transport, film diffusion, intraparticle diffusion, and adsorption attachment. The majority of the time, solution-phase transport occurs swiftly. Hydrodynamic boundary layer/membrane or pore wall diffusion transports the absorbate to the adsorbent's surface or pores. The abundance of binding sites on the MOF surface increases the adsorption rates of Pb(II) and Cd(II). The exchange and sharing of electrons, as well as covalent interactions between metal ions and adsorbent surfaces, impact the chemical adsorption process.

3.4. Adsorption Isotherms

In the current study, isothermal models i.e., Langmuir, Freundlich, Temkin and isotherms were employed to analyze experimental data to better anticipate adsorption removal behaviour and quantify the adsorbent's metal ion adsorption capacity. At a certain temperature, adsorption isotherms describe the relationship between the amount of adsorbate on the adsorbent and the amount of adsorbate in solution at equilibrium. The relevant findings are shown in Fig. 13, and the parameters are listed in Table 5, which unfold that the Langmuir isotherm model agrees with the experimental findings. By comparing the determination coefficient values of both models, Pb(II) and Cd(II) adsorption follow the Langmuir model, which is based on a monolayer sorption onto the surface and a limited number of similar binding sites. The presence of monolayers suggests that pollutants are chemically bonded to the UiO-66-GMA nanoparticles surface (Zhu et al., 2020). Oxygen functional groups on the material's surface resulted in ion-exchange or surface complexion, which led to the formation of chemical bonds with other materials (Zhou et al., 2017). The maximum adsorption capacities for Pb(II) and Cd(II) on UiO-66-GMA were found to be 238.90

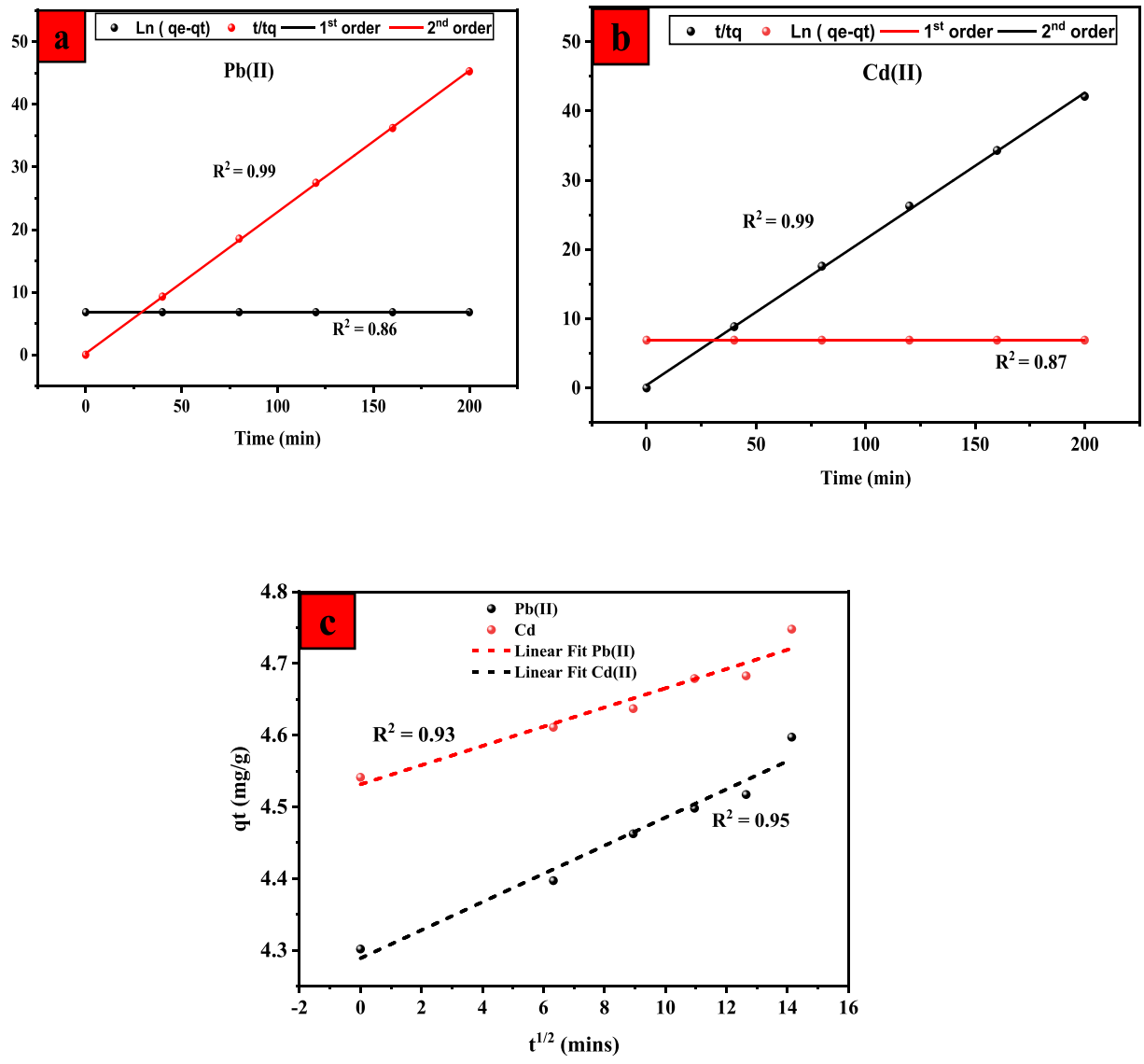

Fig. 12 Adsorption kinetics fitted with Pseudo-first-order, and Pseudo-second-order(a) Pb(II) (b) Cd (II)) and (c) intra-particle diffusion kinetics models.

and 208.33 mg/g, respectively, using the Langmuir isotherm model. Cd(II) ions have a higher adsorption capacity than Pb(II) ions, which may be owing to variations in hydrated radius, electronegativity, acid-base properties, and affinity of UiO-66-GMA nanoparticles.

In the Langmuir adsorption model, RL is an essential parameter showing linear adsorption. The RL parameter has the following criteria: RL greater than 1 indicates unfavourable adsorption, $0 < RL < 1$ indicates favourable adsorption, and $RL = 0$ indicates irreversible adsorption. The calculated RL value is smaller than one, indicating that adsorption is favourable (Khan et al., 2017).

The Temkin adsorption isotherm model studies the relationship between adsorbent and adsorbate, and it is based on the assumption that adsorption heat would not remain constant. The interaction between the adsorbent and the adsorbate reduces it throughout the adsorption process. Adsorption is endothermic, and the negative B values for Pb (II) and Cd(II) imply that chemical sorption is advantageous (Patrulea et al., 2013).

The adsorption process is not represented by the commonly used isotherm models i.e., Langmuir and Freundlich. To do this, the equilibrium data of Pb(II) and Cd(II) ions adsorption onto UiO-66-GMA was examined using the Dubinin-Radushkevich isotherm model (D-R isotherm. It is used to determine the adsorption energy, which indicates the behavior of the adsorption process, either physical or chemical. The non-linear D-R isotherm can be calculated by Eq.(9),(10), and (11).

$$\ln Q_e = \ln Q_m - KE^2 \tag{9}$$

$$\mathbf{E = RTln}\left(1 + \frac{1}{\mathbf{C_e}}\right) \tag{10}$$

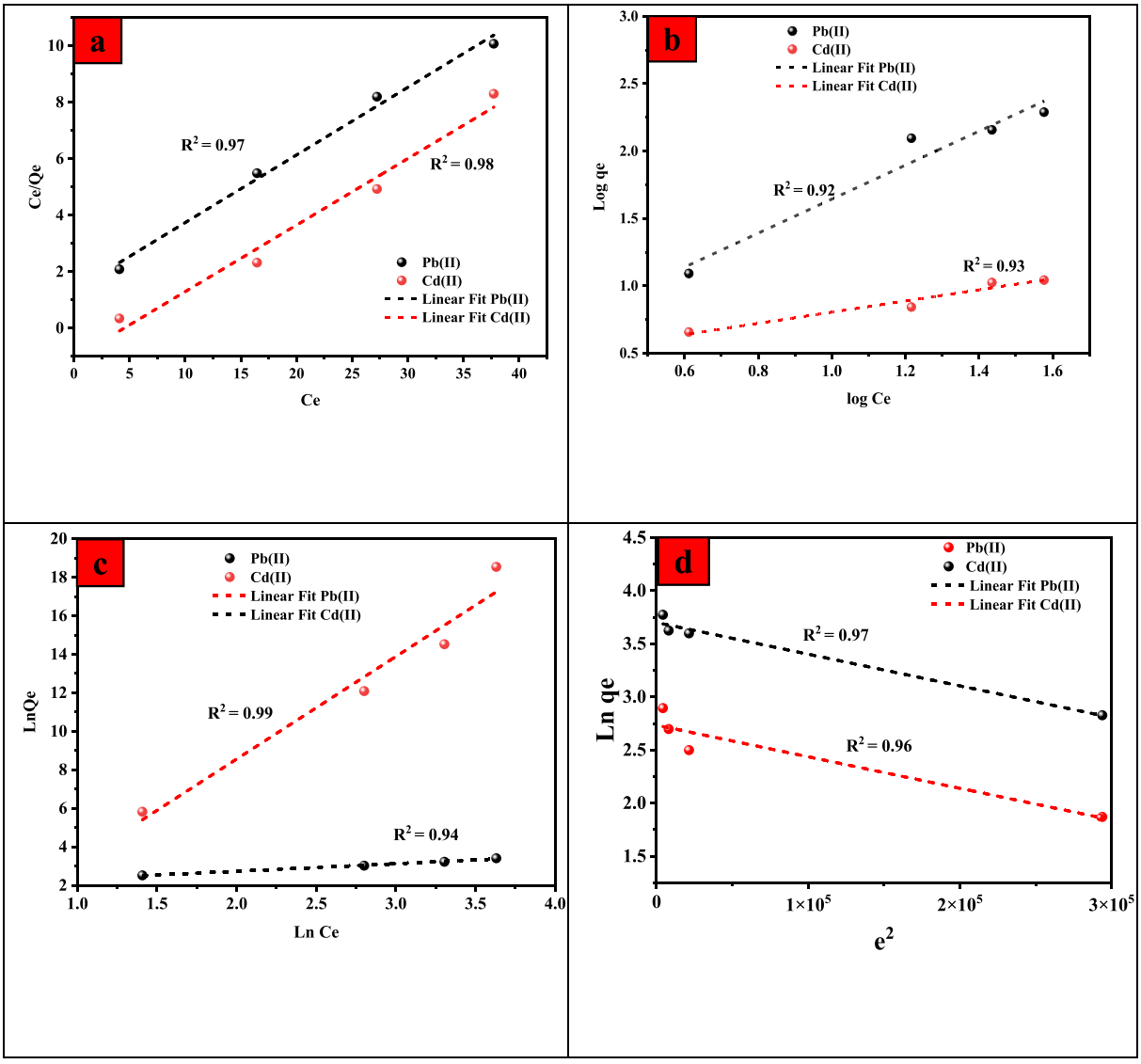

Fig. 13 The adsorption isotherms of Pb(II) and Cd (II) onto UiO-66-GMA, and fitted lines with the (a) Langmuir (b) Freundlich (c) Temkin (d) D-R Isotherm models.

$$\mathbf{E} = \frac{1}{\sqrt{2\mathbf{k}}} \tag{11}$$

where Q_e represents the amount of solute adsorbed, Qm is the maximum adsorption capacity. k and R represent the D-R and gas constant respectively and ε is the Polanyi potential, T (K) is Kelvin temperature and Ce is the equilibrium concentration.

The analyzed parameters are listed in Table 4. The Langmuir model provided the best fit for the experimental data, according to an analysis of the R^2 values obtained using isotherm models. This is due to the fact that the Langmuir model is based on mono molecular layer adsorption, which occurs only on the adsorbent's outer surface, while the D-R model is based on the assumption that the adsorbent pores fill with solute. In Table 6, the mean adsorption free energy (E) values for Pb(II) and Cd(II) ions are more than 8 kJ/mol-1, which suggests that the influence of chemical adsorption will be the dominant factor in the adsorption process of Pb(II) and Cd (II) ions onto the UiO-66-GMA.

Table 4 The kinetic factors for the adsorption of Pb(II) and Cd(II) onto Ui0-66-GMA.

Kinetic models	Metal ions	R^2	K
Pseudo-first-order	Pb(II)	0.86	0.0158
	Cd(II)	0.87	0.005
Pseudo-second-order	Pb(II)	0.99	0.00011
	Cd(II)	0.99	0.00024
Intra-particle diffusion	Pb(II)	0.87	1.795
	Cd(II)	0.89	3.149

3.5. Adsorption Mechanism

Mass transfer occurs by physisorption or chemisorption during the adsorption process. The Pb(II) and Cd(II) ions adsorp-

Table 5 Isotherm parameters for the adsorption removal of Pb(II) and Cd (II) onto the UiO-66-GMA.

	Metals	Freundlich			Langmuir				Temkin			D-R		
		K	n	R^2	KL (L/mg)	Qm (mg/g)	R^2	RL	R^2	B (J/mol)	KT	R^2	E (KJ/mol)	K (mol^2 kJ^{-2})
UiO-66-GMA	Pb(II)	10.90	0.41	0.89	0.356	238.80	0.91	0.24	0.99	−1.64	1.06	0.97	409.576	2.98124E-06
	Cd(II)	10.90	0.4	0.96	0.112	208.45	0.98	0.31	0.99	−1.64	1.04	0.96	401.345	2.7874E-06

Table 6 Thermodynamic parameters for Pb(II) and Cd(II)adsorption onto UiO-66-GMA MOF.

Adsorbent	Heavy Metals	Température (K)	ΔG° (KJ/mol)	ΔH° (KJ/mol)	ΔS° (J/mol K)
UiO-66-GMA	Pb(II)	25	−7.364	229.4	1065.335
		35	−11.258		
		45	−16.069	−63.45	150.76
		55	−19.046		
	Cd(II)	25	1.615	73.44	278.56
		35	2.937		
		45	3.678		
		55	4.978		

tion onto UiO-66-GMA followed pseudo-second-order, and the adsorption process had the characteristic of monolayer adsorption, and the adsorption mode belonged to chemisorption. The adsorption mechanisms for UiO-66-GMA MOF were based on electrostatic interactions, with strong coordination between the Pb(II) and Cd(II) ions and the functional binding groups (e.g., hydroxyl). The binding mechanism between the functional groups and metal ions should be chelate interactions (Wu et al., 2001). Due to electrostatic interaction between the MOF and metal ions fast and maximum Pb (II) and Cd(II) ions adsorption takes place and adsorption mechanism is illustrated in Scheme 2.

By sharing electrons with Pb(II) and Cd(II), the O of the hydroxyl group and the N of NH_2 increased the electron density of nearby carbon atoms and decreased the binding energy of carbon. As a result, the hydroxyl group also played an active role in the electrostatic interaction. Therefore, the interaction of hydroxyl/nitrogen-containing groups with Pb(II) and Cd through electrostatic forces was the mechanism for adsorption. According to the literature, the Zr-MOF operate as a proton donor to encourage strong interactions that bind the metals together (Jamshidifard et al., 2019).

Analysis of the standard free energy (ΔG°, $kJ{\cdot}mol^{-1}$), standard enthalpy (ΔH°, $kJ{\cdot}\ mol^{-1}$), and standard entropy (ΔS°, $J{\cdot}mol^{-1}{\cdot}K^{-1}$) parameters were evaluated using Eq. (12) and (13) for adsorption process inherent energetic changes.

$$\ln\frac{qe}{Ce} = \frac{\Delta S^{o}}{R} - \frac{\Delta H^{o}}{RT} \tag{12}$$

$$\Delta G^{0} = \Delta H^{0} - T\Delta S^{0} \tag{13}$$

where R (8.314 J/mol K) is the gas constant, and T (K) is the temperature in Kelvin.

The negative G° value, as shown in Table 6, indicates that the adsorption process is spontaneous. When the temperature is below 40 °C, the H° and S° values for Pb(II) ions are positive. But at higher temperatures, both H° and S° values negatively show the exothermic adsorption process. As a result, the entropy changes S° at the solution MOF interface increases, which is reflected in the positive entropy value. The results presented In Table 3 demonstrate a negative G°, indicating that the adsorption process is spontaneous. The positive values of H° and S° for Cd(II) indicate an endothermic and entropy-driven adsorption process. When the temperature is below 40 °C, both the H° and S° values for Pb(II) ions are positive. However, above 40 °C, both H° and S° values are negative, suggesting that adsorption processes are exothermic. Furthermore, the positive value of entropy change S° indicates that the unpredictability of Pb(II) ions at the MOF interface has increased. Endothermic reactions between metal ions and the UiO-66-GMA's active sites have been shown to occur, which might also be referred to as the chemical adsorption process.

An Temkin isotherms model was used to better understand the adsorption process of Pb(II) and Cd(II) onto UiO-66-GMA. The reaction is endothermic, as shown in Fig. 13(c), and it is followed by chemical adsorption.

3.6. UiO-66-GMA structural stability

Adsorbent stability is an essential factor to consider while selecting the most cost-effective and acceptable adsorbents for heavy metal ion removal. UiO-66-GMA was tested in HCL (pH = 1) and NaOH (pH = 14) solutions at room temperature to determine its chemical stability. After 24 h of immersion in acidic and basic solutions, XRD patterns reveal good stability, in the both acidic and basic medium as shown in Fig. 14. Wang et al. (2016) identified few MOFs with excellent stability across such a large pH range in aqueous solutions. The Zr_6 cluster is one of the most stable building blocks for MOF synthesis in zirconium. As Zr^{4+} has a high charge density (Z/r) and may polarise the O atoms to produce strong Zr–O bonds with considerable covalent interaction. UiO-66-GMA structure seems to remain nearly unchanged up to pH 14. Due to high structural and chemical stability, the synthesized MOF is well suited for removing metal ions from wastewater.

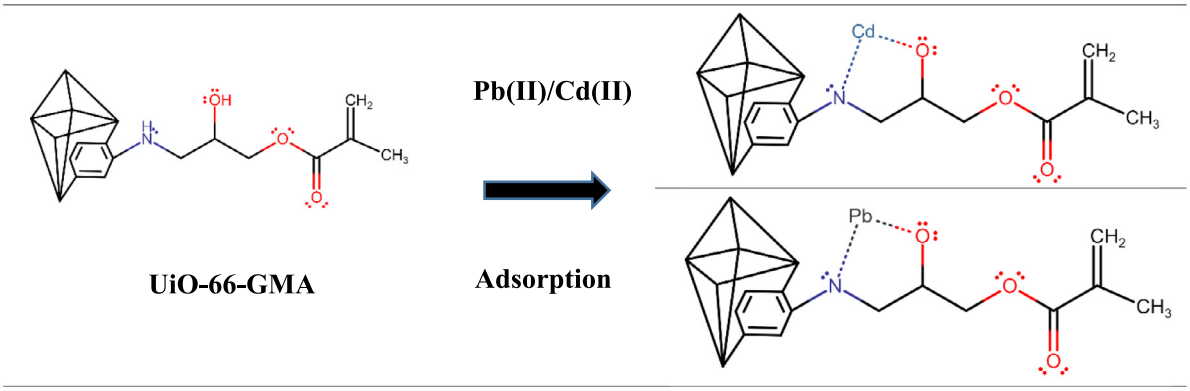

Scheme 2 Adsorption mechanism of Pb(II) and Cd(II) onto UiO-66-GMA.

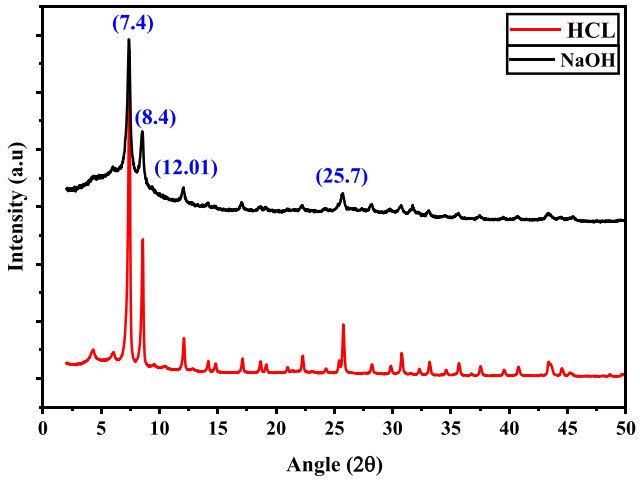

Fig. 14 Structural stability of UiO-66-GMA MOF.

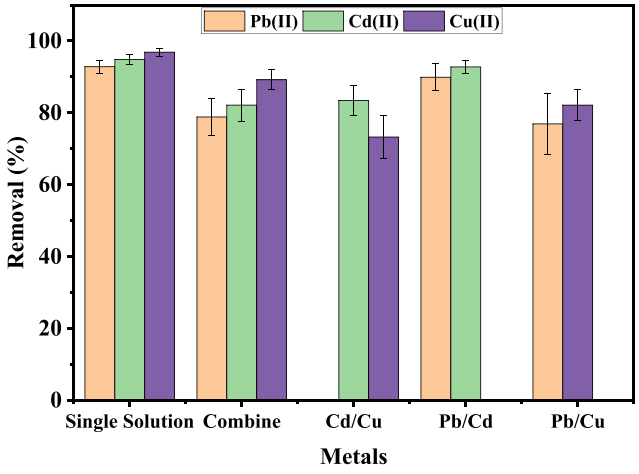

Fig. 15 Effect of multi metal adsorption on the removal efficiency of UiO-66-GMA.

3.7. Multi-Metal Adsorption

The removal effectiveness of UiO-66-GMA in binary (Pb/Cd, Pb/Cu, and Cu/Cd) and ternary (Pb/Cd/Cu) solutions were studied to assess the influence of other metal ions coexisting, as seen in Fig. 15. In binary and ternary solutions, UiO-66-GMA's removal efficiency for all metal ions was reduced. UiO-66-GMA had a removal efficiency of 92.816, 94.81, and 96.87% for Pb(II), Cd(II), and Cu(II) ions in single solutions, respectively. In the ternary solution, the removal efficiency of Pb(II), Cd(II), and Cu(II) are 78.83, 82.123, and 89.2% respectively. Therefore, during adsorption the selectivity of material followed a trend of Cu (II) > Cd (II) > Pb(II) in binary, ternary, and single solutions (II). The ionic radius of the metal ions might be used to explain adsorption trends. Cd(II), Pb(II), and Cu(II) have ionic radii of (0.97 Å), (1.20 Å), (0.73 Å), respectively which indicates that the lower the ionic radius of a metal ion, the higher the adsorption rate. The higher the adsorption rate, the smaller the ionic diameter. Thus, in this study, Cu (II) ions, which have the shortest ionic radii, exhibited the maximum adsorption capacity, followed by Cd (II) and Pb (II) ions (Igwe & Abia, 2007). The hydration energies of the metal ions (DHhyd), which are −2100KJ mol-1 for Cu(II), −1806 KJ mol^{-1} for Cd(II), and −1480 KJ mol^{-1} for Pb(II), also affect the adsorption tendency.

Furthermore, the metal ions hydrolysis reaction could be represented by the equation below; (14).

$$M^{2+} + 2H_20 \rightleftarrows M(OH)_2 + 2H^+ \quad (14)$$

The equation above is a general equation for a two-step reaction, which can be written as;

$$M^{2+} + H_20 \rightleftarrows MOH^+ + H^+ \quad (15)$$

$$MOH^+ + H_20 \rightleftarrows M(OH)_2 + H^+ \quad (16)$$

Adsorption of metal ions on the adsorbent will follow these processes in aqueous solutions. As a consequence, a heavy metal that has been most hydrolyzed will be the least adsorbed. Based on the hydration enthalpies of the metal ions listed above, Pb^{2+} to be hydrolyzed more than Cd^{2+}, then Cu^{2+}, and hence Pb^{2+} to be the least adsorbed and Cu^{2+} to be the most adsorbed on the surface of UiO-66-GMA nanoparticles. The.

3.8. Reusability Study

The reusability of metal-loaded adsorbent was investigated, and the findings are presented in Fig. 16. Regeneration experiments to UiO-66-GMA can use NaOH as the desorbent. First,

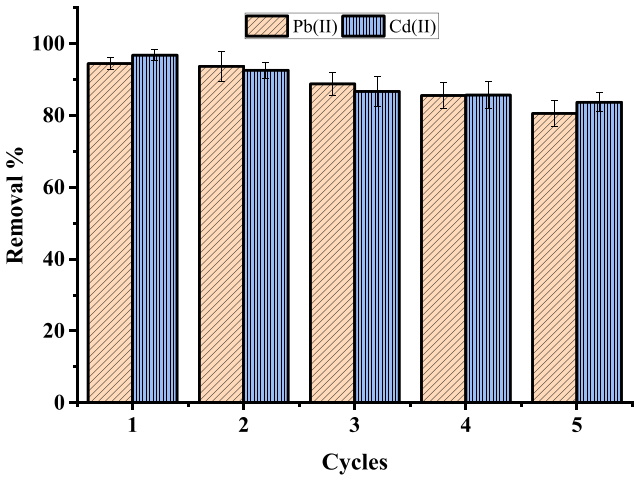

Fig. 16 Performance of the UiO-66-GMA for Pb(II) and Cd(II) removal in five consecutive cycles.

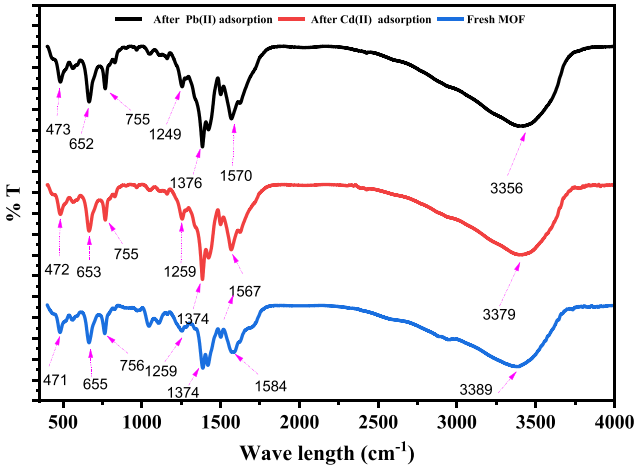

Fig. 17 FT-IR spectra of UiO-66-GMA MOF before and after adsorption.

the adsorbed and saturated UiO-66-GMA was added to 0.1 mol/L (100 mL) of NaOH and agitated for 6 h at room temperature. The desorbed samples were then collected using the suction filtering technique and rinsed with distilled water. In order to reuse the samples in the next round of adsorption studies, they were finally dried in an oven at 70 °C. Five cycles of adsorption regeneration were performed. UiO-66-GMA At low pH levels, there was an increase in Pb(II) and Cd(II) desorption. Using adsorption/desorption cycles, a small decrease in adsorption efficiencies for the synthesized UiO-66-GMA MOF was observed starting with the third cycle, indicating the adsorbent's good reusability. It shows that the regeneration process was completed and that UiO-66-GMA's exhibited high reusability cycling performance and maintained 80.53 %, 83.67% removal efficiency after undergoing five consecutive cycles for Pb(II) and Cd(II) respectively. Monolayer surface adsorption and intraparticle diffusion play a significant role in the removal of Pb(II) and Cd(II) based on an analysis of adsorption kinetics and isotherms.

To further understand the adsorptive processes, the MOFs were studied before and after adsorption. The fresh Ui0-66-GMA MOFs, as shown in Fig. 17, showed similar infrared spectroscopy, and the results are consistent with previous literature (Ramezanzadeh et al., 2021b). In the FTIR spectra, the peak at 3383 cm^{-1} corresponds to the NH_2 stretching vibration. Observed peaks at 1377 and 1257 cm^{-1} correspond to the stretching vibration of C—N. The peak at 1563 cm^{-1} is caused by C—O bonding with Zr (IV). After adsorption of Pb(II) and Cd(II) ions, the stretching vibration of the NH_2 peak was displaced to 3381 cm^{-1} and 3382 cm^{-1}, respectively, and the intensity of C—O, C—N was reduced, indicating that the amino functional group may play a significant role in reacting with Pb(II) and Cd(II) during the adsorption process. Upon adsorption, a drop in band intensity was observed for all of the aforementioned bands, as Pb(II) and Cd(II) coordinated with N in the amine group. Cationic heavy metals can be more effectively removed from MOFs that have been modified to include amino groups in their pores, which results in increased negative zeta potential.

In addition, the XRD patterns of UiO-66-GMA before and after adsorption of Pb(II) and Cd(II) as shown in Fig. 18(a) and (b) verified that no significant decomposition occurred in the framework structure. The structural stability and crys-

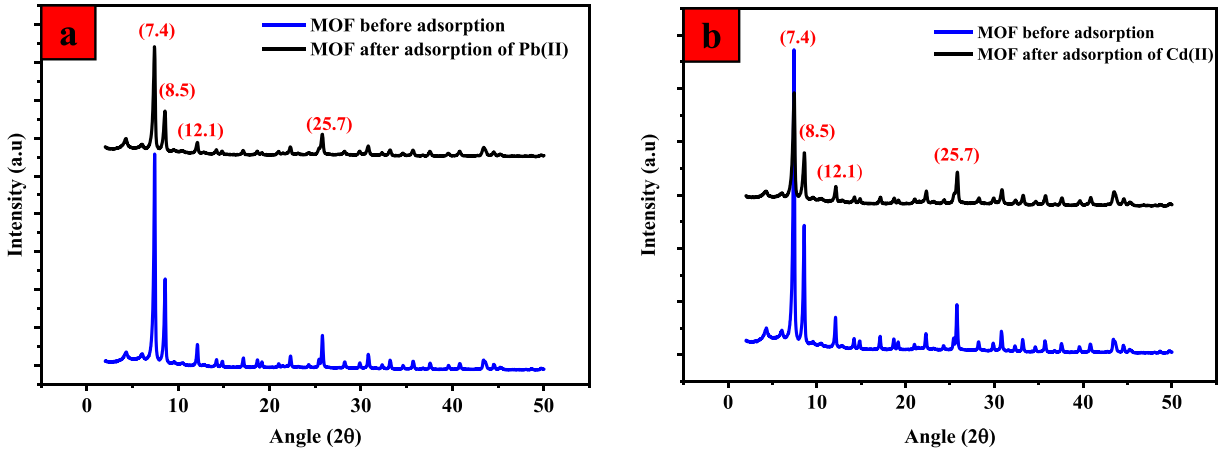

Fig. 18 X-rD spectra of the UiO-66-GMA MOFs before and after adsorption of (a) Pb(II) and (b) Cd II).

Table 7 Comparison of maximum adsorption capacity and synthesis methods for the adsorption of metal ions with the literature.

Sr.No	Adsorbents	Metal ions	Adsorption capacity q_{max}(mg/g)	Synthesis method/ conditions	References
1.	NH_2-Zr-MOF	Pb(II)	166.74	Microwave 5 min 10 h at 80 °C	(Wang et al., 2015)
2.	UiO-66-EDA	Pb (II)	243.90	Solvothermal 36 h 55 °C	(Ahmadijokani et al., 2021)
3.	NH_2-functionalized Zr-MOFs	Pb (II)	50.28	Solvothermal 36 h 55 °C	(Wang et al., 2017)
4.	UiO-66-GMA	Pb(II)	227.80	Microwave 5 min 50 °C	This study
5.	UiO-66-EDA	Cd(II)	217.39	Solvothermal 36 h 55 °C	(Ahmadijokani et al., 2021)
6.	NH_2-functionalized Zr-MOFs	Cd(II)	177.35	Solvothermal 36 h 55 °C	(Wang et al., 2015)
7.	NH_2-TMU-16	Cd(II)	126.6	Solvothermal 36 h 55 °C	(Roushani et al., 2017)
8.	NH_2-functionalized Zr-MOFs	Cd(II)	42.63	Microwave	(Wang et al., 2017)
9.	UiO-66-GMA	Cd(II)	236.45	Microwave 5 min 50 °C	This study

tallinity of MOF before and after adsorption remained unaffected and stable.

3.9. Comparison with previous literature

In the literature, Zr- based MOF has been reported for the adsorption of metals. Table 7 summarizes the maximum adsorption capacity, and synthesis method conditions of Zr-based MOFs towards Pb(II) and Cd(II) metal ions were compared that have been reported in previous studies. The results revealed that MOF were shown to be effective in reducing metal ions levels in aqueous solutions. Previous studies have reported MOF for metal ion adsorption from wastewater; however, limited literature has been found for the Ui0-66-GMA for water treatment. As a result, it is possible to conclude that UiO-66-GMA MOF can effectively adsorb metal ions and probably other contaminants from water.

4. Conclusion

In this study, using microwave heating method, Ui0-66-GMA was synthesized and shows a large surface area, excellent porosity, thermal stability, and reusability. Consequently, the UiO-66-GMA was used as an efficient adsorbent with an adsorption capacity of 238.80 mg/g Pb(II) and 208.45 mg/g Cd(II). The pseudo-second-order kinetic model and the Temkin isotherm model accurately predicted the chemisorption and monolayer adsorption of these metal ions onto UiO-66-GMA. Due to differences in the hydrated radius, electronegativity, and acid-base characteristics of the metals, the UiO-66-GMA selectivity towards them follows the sequence Cd(II) > Pb(II). Furthermore, high temperatures improved UiO-6 6-GMA removal effectiveness. The removal efficiency of UiO-66-GMA for the metal ions studied was significantly influenced by the initial pH of the ion solution. The high removal efficiency of UiO-66-GMA, as well as its excellent structural stability in both neutral and acidic solutions, suggest that this adsorbent might be employed for wastewater treatment. Furthermore, the reusability for both the Pb(II) and Cd(II) metal ions showed that the adsorption efficiency of UiO-66-GMA MOF maintained 80–90 percent even after five cycles. The greater adsorption capacities, desorption efficiencies, and strong structural stability for the removal of metal ions, boost its economic significance.

CRediT authorship contribution statement

Humaira Gul Zaman: Conceptualization, Writing – original draft. **Lavania Baloo:** Conceptualization, Supervision, Funding acquisition. **Shamsul Rahman Kutty:** Supervision. **Muhammad Altaf:** Writing – review & editing.

Declaration of Competing Interest

The authors declare that they have no known competing financial interests or personal relationships that could have appeared to influence the work reported in this paper.

Acknowledgement

Authors are grateful for the financial support provided by Universiti Teknologi PETRONAS via the YUTP grant with cost center 015LCO-303.

References

Abid, H.R., Shang, J., Ang, H.-M., Wang, S., 2013. Amino-functionalized Zr-MOF nanoparticles for adsorption of CO2 and CH4. Int. J. Smart Nano Mater. 4 (1), 72–82.

Ahmadijokani, F., Mohammadkhani, R., Ahmadipouya, S., Shokrgozar, A., Rezakazemi, M., Molavi, H., Arjmand, M., 2020. Superior chemical stability of UiO-66 metal-organic frameworks (MOFs) for selective dye adsorption. Chem. Eng. J. 399, 125346.

Ahmadijokani, F., Tajahmadi, S., Bahi, A., Molavi, H., Rezakazemi, M., Ko, F., Arjmand, M., 2021. Ethylenediamine-functionalized Zr-based MOF for efficient removal of heavy metal ions from water. Chemosphere 264, 128466.

Akpomie, G.K., Abuh, M.A., Ogbu, C.I., Agulanna, A.C., Ekpe, I.O., 2012. Adsorption of Cd (II) from solution by nsu clay: kinetic and

thermodynamic studies. J. Emerg. Trends Eng. Appl. Sci. 3 (2), 254–258.
Atia, A.A., Donia, A.M., Yousif, A.M., 2005. Comparative study of the recovery of silver (I) from aqueous solutions with different chelating resins derived from glycidyl methacrylate. J. Appl. Polym. Sci. 97 (3), 806–812.
Badruddoza, A.Z.M., Shawon, Z.B.Z., Tay, W.J.D., Hidajat, K., Uddin, M.S., 2013. Fe3O4/cyclodextrin polymer nanocomposites for selective heavy metals removal from industrial wastewater. Carbohydr. Polym. 91 (1), 322–332.
Bhattacharyya, K.G., Gupta, S.S., 2007. Adsorptive accumulation of Cd (II), Co (II), Cu (II), Pb (II), and Ni (II) from water on montmorillonite: Influence of acid activation. J. Colloid Interface Sci. 310 (2), 411–424.
Cao, Y., Zhang, H., Song, F., Huang, T., Ji, J., Zhong, Q., Xu, Q., 2018. UiO-66-NH2/GO composite: synthesis, characterization and CO2 adsorption performance. Materials 11 (4), 589.
Carpio, I.E.M., Mangadlao, J.D., Nguyen, H.N., Advincula, R.C., Rodrigues, D.F., 2014. Graphene oxide functionalized with ethylenediamine triacetic acid for heavy metal adsorption and anti-microbial applications. Carbon 77, 289–301.
Cavka, J.H., Jakobsen, S., Olsbye, U., Guillou, N., Lamberti, C., Bordiga, S., Lillerud, K.P., 2008. A new zirconium inorganic building brick forming metal organic frameworks with exceptional stability. J. Am. Chem. Soc. 130 (42), 13850–13851.
Chavan, S., Vitillo, J.G., Gianolio, D., Zavorotynska, O., Civalleri, B., Jakobsen, S., Lillerud, K.P., 2012. H 2 storage in isostructural UiO-67 and UiO-66 MOFs. PCCP 14 (5), 1614–1626.
Chen, Q., He, Q., Lv, M., Xu, Y., Yang, H., Liu, X., Wei, F., 2015. Selective adsorption of cationic dyes by UiO-66-NH2. Appl. Surf. Sci. 327, 77–85.
Demiral, H., Güngör, C., 2016. Adsorption of copper (II) from aqueous solutions on activated carbon prepared from grape bagasse. J. Cleaner Prod. 124, 103–113.
Dennis, G., Harrison, W., Agnes, K., Erastus, G., 2016. Effect of biological control antagonists adsorbed on chitosan immobilized silica nanocomposite on Ralstonia solanacearum and growth of tomato seedlings. Adv. Res., 1–23
Dou, X.B., Chai, M.Y., Zhu, Y., Yang, W.T., Xu, F.J., 2013. Aminated poly (glycidyl methacrylate) s for constructing efficient gene carriers. ACS Appl. Mater. Interfaces 5 (8), 3212–3218.
Feng, D., Gu, Z.Y., Li, J.R., Jiang, H.L., Wei, Z., Zhou, H.C., 2012. Zirconium-metalloporphyrin PCN-222: mesoporous metal–organic frameworks with ultrahigh stability as biomimetic catalysts. Angew. Chem. Int. Ed. 51 (41), 10307–10310.
Fiaz, M., Athar, M., 2020. Enhancing the hydrogen and oxygen evolution reaction efficiency of amine functionalized MOF NH2-UiO-66 via incorporation of CuO nanoparticles. Catal. Lett. 150 (11), 3314–3326.
Guilane, S., Hamdaoui, O., 2016. Regeneration of exhausted granular activated carbon by low frequency ultrasound in batch reactor. Desalin. Water Treat. 57 (34), 15826–15834.
Hasan, Z., Khan, N.A., Jhung, S.H., 2016. Adsorptive removal of diclofenac sodium from water with Zr-based metal–organic frameworks. Chem. Eng. J. 284, 1406–1413.
He, X., Deng, F., Shen, T., Yang, L., Chen, D., Luo, J., Wang, F., 2019. Exceptional adsorption of arsenic by zirconium metal-organic frameworks: engineering exploration and mechanism insight. J. Colloid Interface Sci. 539, 223–234.
Hur, J., Shin, J., Yoo, J., Seo, Y.-S., 2015. Competitive adsorption of metals onto magnetic graphene oxide: comparison with other carbonaceous adsorbents. Sci. World J. 2015.
Hussain Qaiser, M.S., Ahmad, I., Ahmad, S.R., Afzal, M., Qayyum, A., 2019. Assessing Heavy Metal Contamination in Oil and Gas Well Drilling Waste and Soil in Pakistan. Polish J. Environ. Stud. 28 (2).
Hwang, Y.K., Hong, D.Y., Chang, J.S., Jhung, S.H., Seo, Y.K., Kim, J., Férey, G., 2008. Amine grafting on coordinatively unsaturated metal centers of MOFs: consequences for catalysis and metal encapsulation. Angew. Chem. 120 (22), 4212–4216.
Igwe, J.C., Abia, A.A., 2007. Adsorption isotherm studies of Cd (II), Pb (II) and Zn (II) ions bioremediation from aqueous solution using unmodified and EDTA-modified maize cob. Eclética Química 32 (1), 33–42.
Jamshidifard, S., Koushkbaghi, S., Hosseini, S., Rezaei, S., Karamipour, A., Irani, M., 2019. Incorporation of UiO-66-NH2 MOF into the PAN/chitosan nanofibers for adsorption and membrane filtration of Pb (II), Cd (II) and Cr (VI) ions from aqueous solutions. J. Hazard. Mater. 368, 10–20.
Jiao, C., Xiong, J., Tao, J., Xu, S., Zhang, D., Lin, H., Chen, Y., 2016. Sodium alginate/graphene oxide aerogel with enhanced strength–toughness and its heavy metal adsorption study. Int. J. Biol. Macromol. 83, 133–141.
Kalmykova, Y., Strömvall, A.-M., Steenari, B.-M., 2008. Adsorption of Cd, Cu, Ni, Pb and Zn on Sphagnum peat from solutions with low metal concentrations. J. Hazard. Mater. 152 (2), 885–891.
Khan, T., Mustafa, M.R.U., Isa, M.H., Abd Manan, T.S.B., Ho, Y.-C., Lim, J.-W., Yusof, N.Z., 2017. Artificial neural network (ANN) for modelling adsorption of lead (Pb (II)) from aqueous solution. Water Air Soil Pollut. 228 (11), 1–15.
Kim, M., Cahill, J.F., Fei, H., Prather, K.A., Cohen, S.M., 2012. Postsynthetic ligand and cation exchange in robust metal–organic frameworks. J. Am. Chem. Soc. 134 (43), 18082–18088.
Klinowski, J., Paz, F.A.A., Silva, P., Rocha, J., 2011. Microwave-assisted synthesis of metal–organic frameworks. Dalton Trans. 40 (2), 321–330.
Kobielska, P.A., Howarth, A.J., Farha, O.K., Nayak, S., 2018. Metal–organic frameworks for heavy metal removal from water. Coord. Chem. Rev. 358, 92–107.
Kopinke, F.-D., Georgi, A., Goss, K.-U., 2018. Comment on "Mistakes and inconsistencies regarding adsorption of contaminants from aqueous solution: A critical review, published by Tran et al.[Water Research 120, 2017, 88–116]". Water Res. 129, 520–521.
Liu, X., Pang, H., Liu, X., Li, Q., Zhang, N., Mao, L., Wang, X., 2021. Orderly porous covalent organic frameworks-based materials: superior adsorbents for pollutants removal from aqueous solutions. The Innovation 2 (1), 100076.
Mahmoud, M.E., Amira, M.F., Azab, M.M.H.M., Abdelfattah, A.M., 2021. Effective removal of levofloxacin drug and Cr (VI) from water by a composed nanobiosorbent of vanadium pentoxide@ chitosan@ MOFs. Int. J. Biol. Macromol. 188, 879–891.
Mahmoud, M.E., Mohamed, A.K., 2020. Novel derived pectin hydrogel from mandarin peel based metal-organic frameworks composite for enhanced Cr (VI) and Pb (II) ions removal. Int. J. Biol. Macromol. 164, 920–931.
Mansouri, M., Sadeghian, S., Mansouri, G., Setareshenas, N., 2021. Enhanced photocatalytic performance of UiO-66-NH2/TiO2 composite for dye degradation. Environ. Sci. Pollut. Res. 28 (20), 25552–25565.
Mishra, P., Islam, M., Patel, R., 2013. Removal of lead (II) by chitosan from aqueous medium. Sep. Sci. Technol. 48 (8), 1234–1242.
Mohamed, A.K., Mahmoud, M.E., 2020. Encapsulation of starch hydrogel and doping nanomagnetite onto metal-organic frameworks for efficient removal of fluvastatin antibiotic from water. Carbohydr. Polym. 245, 116438.
Molavi, H., Eskandari, A., Shojaei, A., Mousavi, S.A., 2018a. Enhancing CO2/N2 adsorption selectivity via post-synthetic modification of NH2-UiO-66 (Zr). Microporous Mesoporous Mater. 257, 193–201.
Molavi, H., Hakimian, A., Shojaei, A., Raeiszadeh, M., 2018b. Selective dye adsorption by highly water stable metal-organic

framework: Long term stability analysis in aqueous media. Appl. Surf. Sci. 445, 424–436.
Molavi, H., Joukani, F.A., Shojaei, A., 2018c. Ethylenediamine grafting to functionalized NH2–UiO-66 using green aza-michael addition reaction to improve CO2/CH4 adsorption selectivity. Ind. Eng. Chem. Res. 57 (20), 7030–7039.
Molavi, H., Shojaei, A., Mousavi, S.A., 2018d. Improving mixed-matrix membrane performance via PMMA grafting from functionalized NH 2–UiO-66. J. Mater. Chem. A 6 (6), 2775–2791.
Molavi, H., Shojaei, A., Pourghaderi, A., 2018e. Rapid and tunable selective adsorption of dyes using thermally oxidized nanodiamond. J. Colloid Interface Sci. 524, 52–64.
Nik, O.G., Chen, X.Y., Kaliaguine, S., 2012. Functionalized metal organic framework-polyimide mixed matrix membranes for CO2/CH4 separation. J. Membr. Sci. 413, 48–61.
Nong, W., Liu, X., Wang, Q., Wu, J., Guan, Y., 2020. Metal-organic framework-based materials: synthesis, stability and applications in food safety and preservation. ES Food Agroforest. 1 (10), 11–40.
Nyairo, W.N., Eker, Y.R., Kowenje, C., Akin, I., Bingol, H., Tor, A., Ongeri, D.M., 2018. Efficient adsorption of lead (II) and copper (II) from aqueous phase using oxidized multiwalled carbon nanotubes/polypyrrole composite. Sep. Sci. Technol. 53 (10), 1498–1510.
Patrulea, V., Negrulescu, A., Mincea, M.M., Pitulice, L.D., Spiridon, O.B., Ostafe, V., 2013. Optimization of the removal of copper (II) ions from aqueous solution on chitosan and cross-linked chitosan beads. BioResources 8 (1), 1147–1165.
Phuengprasop, T., Sittiwong, J., Unob, F., 2011. Removal of heavy metal ions by iron oxide coated sewage sludge. J. Hazard. Mater. 186 (1), 502–507.
Qin, Q., Wang, Q., Fu, D., Ma, J., 2011. An efficient approach for Pb (II) and Cd (II) removal using manganese dioxide formed in situ. Chem. Eng. J. 172 (1), 68–74.
Rallapalli, P., Prasanth, K.P., Patil, D., Somani, R.S., Jasra, R.V., Bajaj, H.C., 2011. Sorption studies of CO 2, CH 4, N 2, CO, O 2 and Ar on nanoporous aluminum terephthalate [MIL-53 (Al)]. J. Porous Mater. 18 (2), 205–210.
Ramezanzadeh, M., Ramezanzadeh, B., Bahlakeh, G., Tati, A., Mahdavian, M., 2021a. Development of an active/barrier bi-functional anti-corrosion system based on the epoxy nanocomposite loaded with highly-coordinated functionalized zirconium-based nanoporous metal-organic framework (Zr-MOF). Chem. Eng. J. 408, 127361.
Ramezanzadeh, M., Tati, A., Bahlakeh, G., Ramezanzadeh, B., 2021b. Construction of an epoxy composite coating with exceptional thermo-mechanical properties using Zr-based NH2-UiO-66 metal-organic framework (MOF): Experimental and DFT-D theoretical explorations. Chem. Eng. J. 408, 127366.
Rezakazemi, M., Amooghin, A.E., Montazer-Rahmati, M.M., Ismail, A.F., Matsuura, T., 2014. State-of-the-art membrane based CO2 separation using mixed matrix membranes (MMMs): An overview on current status and future directions. Prog. Polym. Sci. 39 (5), 817–861.
Roushani, M., Saedi, Z., Baghelani, Y.M., 2017. Removal of cadmium ions from aqueous solutions using TMU-16-NH2 metal organic framework. Environ. Nanotechnol. Monit. Manage. 7, 89–96.
Saleem, H., Rafique, U., Davies, R.P., 2016. Investigations on post-synthetically modified UiO-66-NH2 for the adsorptive removal of heavy metal ions from aqueous solution. Microporous Mesoporous Mater. 221, 238–244.
Sanchez, C., Belleville, P., Popall, M., Nicole, L., 2011. Applications of advanced hybrid organic–inorganic nanomaterials: from laboratory to market. Chem. Soc. Rev. 40 (2), 696–753.
Sarker, M., Song, J.Y., Jhung, S.H., 2018. Carboxylic-acid-functionalized UiO-66-NH2: a promising adsorbent for both aqueous-and non-aqueous-phase adsorptions. Chem. Eng. J. 331, 124–131.
Shi, Z., Xu, C., Guan, H., Li, L., Fan, L., Wang, Y., Zhang, R., 2018. Magnetic metal organic frameworks (MOFs) composite for removal of lead and malachite green in wastewater. Colloids Surf. A 539, 382–390.
Soltani, R., Pelalak, R., Pishnamazi, M., Marjani, A., Albadarin, A.B., Sarkar, S.M., Shirazian, S., 2021. A novel and facile green synthesis method to prepare LDH/MOF nanocomposite for removal of Cd (II) and Pb (II). Sci. Rep. 11 (1), 1–15.
Tannert, N., Gökpinar, S., Hastürk, E., Nießing, S., Janiak, C., 2018. Microwave-assisted dry-gel conversion-a new sustainable route for the rapid synthesis of metal–organic frameworks with solvent re-use. Dalton Trans. 47 (29), 9850–9860.
Thornton, A.W., Nairn, K.M., Hill, J.M., Hill, A.J., Hill, M.R., 2009. Metal− organic frameworks impregnated with magnesium-decorated fullerenes for methane and hydrogen storage. J. Am. Chem. Soc. 131 (30), 10662–10669.
Tian, P., He, X., Li, W., Zhao, L., Fang, W., Chen, H., Wang, W., 2018. Zr-MOFs based on Keggin-type polyoxometalates for photocatalytic hydrogen production. J. Mater. Sci. 53 (17), 12016–12029.
Truong, T., Dang, G.H., Tran, N.V., Truong, N.T., Le, D.T., Phan, N.T.S., 2015. Oxidative cross-dehydrogenative coupling of amines and α-carbonyl aldehydes over heterogeneous Cu-MOF-74 catalyst: A ligand-and base-free approach. J. Mol. Catal. A: Chem. 409, 110–116.
Vasconcelos, H.L., Fávere, V.T., Gonçalves, N.S., Laranjeira, M.C. M., 2007. Chitosan modified with Reactive Blue 2 dye on adsorption equilibrium of Cu (II) and Ni (II) ions. React. Funct. Polym. 67 (10), 1052–1060.
Wang, H., Dong, X., Lin, J., Teat, S.J., Jensen, S., Cure, J., Wang, Q., 2018. Topologically guided tuning of Zr-MOF pore structures for highly selective separation of C6 alkane isomers. Nat. Commun. 9 (1), 1–11.
Wang, K., Gu, J., Yin, N., 2017. Efficient removal of Pb (II) and Cd (II) using NH2-functionalized Zr-MOFs via rapid microwave-promoted synthesis. Ind. Eng. Chem. Res. 56 (7), 1880–1887.
Wang, B., Lv, X.-L., Feng, D., Xie, L.-H., Zhang, J., Li, M., Zhou, H.-C., 2016. Highly stable Zr (IV)-based metal–organic frameworks for the detection and removal of antibiotics and organic explosives in water. J. Am. Chem. Soc. 138 (19), 6204–6216.
Wang, L., Xing, R., Liu, S., Yu, H., Qin, Y., Li, K., Li, P., 2010a. Recovery of silver (I) using a thiourea-modified chitosan resin. J. Hazard. Mater. 180 (1–3), 577–582.
Wang, L., Yang, L., Li, Y., Zhang, Y., Ma, X., Ye, Z., 2010b. Study on adsorption mechanism of Pb (II) and Cu (II) in aqueous solution using PS-EDTA resin. Chem. Eng. J. 163 (3), 364–372.
Wang, Y., Ye, G., Chen, H., Hu, X., Niu, Z., Ma, S., 2015. Functionalized metal–organic framework as a new platform for efficient and selective removal of cadmium (II) from aqueous solution. J. Mater. Chem. A 3 (29), 15292–15298.
Wang, L., Zhang, J., Zhao, R., Li, Y., Li, C., Zhang, C., 2010c. Adsorption of Pb (II) on activated carbon prepared from Polygonum orientale Linn.: kinetics, isotherms, pH, and ionic strength studies. Bioresour. Technol. 101 (15), 5808–5814.
Wang, X.S., Zhou, Y., Jiang, Y., Sun, C., 2008. The removal of basic dyes from aqueous solutions using agricultural by-products. J. Hazard. Mater. 157 (2–3), 374–385.
Wißmann, G., Schaate, A., Lilienthal, S., Bremer, I., Schneider, A.M., Behrens, P., 2012. Modulated synthesis of Zr-fumarate MOF. Microporous Mesoporous Mater. 152, 64–70.
Wu, S., Ge, Y., Wang, Y., Chen, X., Li, F., Xuan, H., Li, X., 2018. Adsorption of Cr (VI) on nano Uio-66-NH2 MOFs in water. Environ. Technol. 39 (15), 1937–1948.
Wu, F.-C., Tseng, R.-L., Juang, R.-S., 2001. Kinetic modeling of liquid-phase adsorption of reactive dyes and metal ions on chitosan. Water Res. 35 (3), 613–618.

Xiong, C., Wang, S., Zhang, L., Li, Y., Zhou, Y., Peng, J., 2018. Selective recovery of silver from aqueous solutions by poly (glycidyl methacrylate) microsphere modified with trithiocyanuric acid. J. Mol. Liq. 254, 340–348.

Yaghi, O.M., Li, G., Li, H., 1995. Selective binding and removal of guests in a microporous metal–organic framework. Nature 378 (6558), 703–706.

Yaghi, O.M., O'Keeffe, M., Ockwig, N.W., Chae, H.K., Eddaoudi, M., Kim, J., 2003. Reticular synthesis and the design of new materials. Nature 423 (6941), 705–714.

Yan, J., Lan, G., Qiu, H., Chen, C., Liu, Y., Du, G., Zhang, J., 2018. Adsorption of heavy metals and methylene blue from aqueous solution with citric acid modified peach stone. Sep. Sci. Technol. 53 (11), 1678–1688.

Yang, Z., Tong, X., Feng, J., He, S., Fu, M., Niu, X., Feng, X., 2019. Flower-like BiOBr/UiO-66-NH2 nanosphere with improved photocatalytic property for norfloxacin removal. Chemosphere 220, 98–106.

Yin, X.C., Liu, X., Fan, J.C., Wu, J.J., Men, J.L., Zheng, G.S., 2017. Preparation of gel resins and removal of copper and lead from water. J. Appl. Polym. Sci. 134 (7).

Younas, M., Rezakazemi, M., Daud, M., Wazir, M.B., Ahmad, S., Ullah, N., Ramakrishna, S., 2020. Recent progress and remaining challenges in post-combustion CO2 capture using metal-organic frameworks (MOFs). Prog. Energy Combust. Sci. 80, 100849.

Yuan, S., Zhang, J., Yang, Z., Tang, S., Liang, B., Pehkonen, S.O., 2017. Click functionalization of poly (glycidyl methacrylate) microspheres with triazole-4-carboxylic acid for the effective adsorption of Pb (II) ions. New J. Chem. 41 (14), 6475–6488.

Zhang, X., Yan, L., Li, J., Yu, H., 2020. Adsorption of heavy metals by l-cysteine intercalated layered double hydroxide: kinetic, isothermal and mechanistic studies. J. Colloid Interface Sci. 562, 149–158.

Zhou, N., Chen, H., Feng, Q., Yao, D., Chen, H., Wang, H., Lu, X., 2017. Effect of phosphoric acid on the surface properties and Pb (II) adsorption mechanisms of hydrochars prepared from fresh banana peels. J. Cleaner Prod. 165, 221–230.

Zhu, L., Shen, D., Luo, K.H., 2020. A critical review on VOCs adsorption by different porous materials: Species, mechanisms and modification methods. J. Hazard. Mater. 389, 122102.

Zhu, J., Wu, L., Bu, Z., Jie, S., Li, B.-G., 2019. Polyethyleneimine-modified UiO-66-NH2 (Zr) metal–organic frameworks: preparation and enhanced CO2 selective adsorption. ACS Omega 4 (2), 3188–3197.